



The Impact of Atmospheric and Tectonic Constraints on Radon-222 and Carbon Dioxide Flow in Geological Porous Media - A Dozen-Year Research Summary

Hovav Zafrir^{1,2*}, Susana Barbosa³, Elad Levintal⁴, Noam Weisbrod⁴, Yochai Ben Horin⁵ and Zeev Zalevsky¹

OPEN ACCESS

Edited by:

Giovanni Martinelli,
National Institute of Geophysics and
Volcanology, Section of Palermo, Italy

Reviewed by:

Vivek Wallia,
National Center for Research on
Earthquake Engineering, Taiwan
Heiko Woith,
German Research Centre for
Geosciences, Helmholtz Centre
Potsdam, Germany

*Correspondence:

Hovav Zafrir
hzafrir@gmail.com

Specialty section:

This article was submitted to
Geochemistry,
a section of the journal
Frontiers in Earth Science

Received: 05 May 2020

Accepted: 07 September 2020

Published: 30 October 2020

Citation:

Zafrir H, Barbosa S, Levintal E,
Weisbrod N, Ben Horin Y and Zalevsky
Z (2020) The Impact of Atmospheric
and Tectonic Constraints on Radon-
222 and Carbon Dioxide Flow in
Geological Porous Media - A Dozen-
Year Research Summary.
Front. Earth Sci. 8:559298.
doi: 10.3389/feart.2020.559298

¹ Faculty of Engineering, Bar Ilan University, Ramat-Gan, Israel, ² Geological Survey of Israel, Jerusalem, Israel, ³ INESC TEC, Porto, Portugal, ⁴ The Jacob Blaustein Institutes for Desert Research, Ben Gurion University of the Negev, Midreshet Ben Gurion, Israel, ⁵ Soreq Nuclear Research Center, Yavne, Israel

Long-term monitoring of Rn-222 and CO₂ at a depth of several dozen meter at the Sde-Eliezer site, located within one of the Dead Sea Fault Zone segments in northern Israel, has led to the discovery of the clear phenomenon that both gases are affected by underground tectonic activity along the Dead Sea Fault Zone. It may relate to pre-seismic processes associated with the accumulation and relaxation of lithospheric stress and strain producing earthquakes. This approach assumes that meteorological influences on physico-chemical parameters are limited at depth since its strength diminishes with the increase of the overlay layer thickness. Hence, the monitoring of natural gases in deep boreholes above the water table enables to reduce the climatic-induced periodic contributions, and thus to identify the specific portion of the radon signals that could be related to regional tectonic pre-seismic activity. The plausible pre-seismic local movement of the two gases at depth - is identified by the appearance of discrete, random, non-cyclical signals, wider in time duration than 20 h and clearly wider than the sum of the width of the periodic diurnal and semidiurnal signals driven by ambient meteorological parameters. These non-cyclical signals may precede, by one day or more, a forthcoming seismic event. Hence, it is plausible to conclude that monitoring of any other natural gas that is present at depth may show a similar broadening signal and may serve as a precursor too. The necessary technical conditions enabling to distinguish between anomalous signals of gases that may be induced locally by pre-seismic processes at depth, and the relatively low periodic signals that are still established at depth related to external climatic conditions, are presented in detail.

Keywords: radon monitoring, thermal flow in porous media, earthquake precursors, borehole monitoring, barometric pumping

INTRODUCTION

Overview

Previous research on radon has been carried out in the last 45 years in various geological environments such as soil (e.g., Akerblom et al., 1984; Schubert and Schultz, 2002; Fujiyoshi et al., 2006; Muga, 2017; Cannelli et al., 2018; Siino et al., 2019), solid rocks (e.g., Vulkan et al., 1992; Steinitz et al., 2007; Barbosa et al., 2010), fans of erosion streams (e.g., Steinitz et al., 1992), subterranean structures such as caves, tunnels and mines (e.g., Hakl et al., 1996; Przylibski, 2001; Muramatsu et al., 2002; Cigna, 2005; Richon et al., 2005; Mentés and Eper-Pápai, 2015; Sahu et al., 2016) and groundwater (e.g., Igarashi et al., 1995; Atkins et al., 2016; Barberio et al., 2018). The main objective of such studies was either to examine the association between radon concentration changes in shallow surface environments and the health risk of radon in augmenting lung cancer, or to investigate the connection between radon and geodynamics (e.g., Mogro-Campero et al., 1977; Fleischer, 1981; Monnin et al., 1993; Trique et al., 1999; Steinitz et al., 2003; Zafrir et al., 2003; Groves-Kirkby et al., 2004; Cicerone et al., 2009; Ghosh et al., 2009; Vaupotič et al., 2010; Oh and Kim, 2015; Riggio et al., 2015; Zafrir et al., 2016; Fu et al., 2017; Singh et al., 2017) and volcanic eruptions (e.g., Eff-Darwich et al., 2002; Martín-Luis et al., 2015; Falsaperla et al., 2017; Torres-Gonzalez et al., 2019).

The available techniques for the measurement of radon and its decay products (RDPs) in sub-ground media are based on the interaction of either alpha particles or gamma-rays with the sensor material. The most common means for the measurement of radon is through the detection of alpha particle emission from the decay of Rn-222 (5.49 MeV), Po-218 (6.00 MeV) and Po-214 (7.69 MeV), or gamma ray radiation from radon decay products (RDPs) mainly Bi-214 and Pb-214 (e.g., Ivanovich and Harmon, 1982). The detection process includes recording of the alpha or gamma radiation for sequential time intervals (seconds to hours). Electronic automatic radon monitoring station are known to be operated in diverse places such as Japan (e.g., Noguchi and Wakita, 1977), China (e.g., King, 1986), and Europe (e.g., Koch and Heinicke, 1994). Most of these stations measure radon in water or soil using either Lucas cells (based on ZnS for detection of alpha particles) or NaI (for gamma detection).

A wide variety of measuring methods are presented in the literature (e.g., Knoll, 2000). For example, for passive detection, activated charcoal that adsorbs radon and its decay products from air (e.g., George, 1984) and alpha-sensitive CR-39 or LR-115 nuclear track films (e.g., Fleischer et al., 1984; Jönsson, 1997; Wertheim et al., 2010). Sealed metal cells covered with scintillator as zinc sulphide (Lucas cells, Lucas, 1957) used to measure pumped radon samples as well as ionization chambers (e.g., Ichitsubo and Yamada, 2004), and silicon photodiodes (e.g., George, 1990). Gamma sensors including Geiger-Mueller counters, scintillation light detection devices (e.g., Vulkan et al., 1995; Walia et al., 2005; Zafrir et al., 2009; Zafrir et al., 2011) and silicon photodiodes (e.g., Pinault and Baubron, 1996), have been exploited during the last 30 years, for radon detection.

In continuous long-term radon measurements, the mandatory essential condition is not to violate the natural thermodynamic equilibrium nor the radon and RDPs secular equilibrium, by pumping and grabbing radon samples from the geological porous media below the surface. The measurement technologies that allow working in passive mode are the alpha-particles sensors based on silicon photodiodes or ionization chambers, and gamma detectors based on various scintillation materials. It enables tracking temporal radon fluctuations under natural stable internal conditions, with a high-resolution sampling rate from once every few seconds up to several minutes.

For radon measurement by alpha detectors, the prime concealed problem is the ability of radon gas to move out from the solid grain to the intergranular space in the bedrock (emanation), and then to flow out to the air space (exhalation) in order to be perceived and measured by the detector. By taking into consideration that less than 32 percent of the radon content in rock emanate from the solid grains to the porous media (Hassan et al., 2009) and that the radon exhalation greatly depends on the features of the investigated media, such as its thickness, the internal structure as well as the moisture content of the solid phase, the amount of the radon gas being exhaled to the air and that may temporally be detected is less than 10%.

In addition, when an alpha detector is set inside a borehole, for example, it has to respond to radon particles that first have to enter by diffusion from the air space into the detector's sensing volume (dozens of cm³). Then the alpha radiation which is emitted by the Rn-222 and its RDPs, Po-218 and Po-214, has to reach the internal silicon solid state sensor to produce counting signals. This process greatly reduces the efficiency of the measurement.

On the other side, there is an intrinsic distinction between the alpha and the gamma measurement, related to the sensing capabilities. When a gamma detector is installed, inside a borehole, within a geological formation, it responds to the radon existing within a surrounding spherical body of bedrocks of a radius of $R + 35$ cm (where R is the borehole radii and the 35 cm is the average gamma absorption length). In addition to the three-scale difference in the size of sensing volume, the gamma detection method enables principally the measurement of radon content directly inside the country rock media. Thus, it is the ideal passive method for measuring radon concentration under natural and undisturbed conditions, suitable for resolving small temporal changes provided that the gamma detectors have high detection sensitivity which is essential to distinguish between minor variations in amplitudes and time.

In light of the above, it is possible to summarize in general the important requirements to be taken into account in choosing radon detection systems for long-time monitoring as follows:

- The ability to discern small changes in the intensity of measured signals high resolution capability with high signal to noise ratio
- The ability to discern small changes in the variability of the signals at a high level of time separation, at a measurement rate of at least a few seconds high temporal resolution

- Reliability in measurements over time—a stable measurement capacity for months to years
- Automatic data collection and remote data transmission

The rules listed above rule out the use for long-time radon monitoring of the techniques based on alpha particles detection by nuclear track films or active charcoal, or even radon extraction and grabbing from subsurface soil or rocks into ionization or Lucas cells, since the results are not continuous, the measurement times are too long, and the devices may reach saturation. Radon monitoring ionization chambers and silicon photodiodes-based alpha particle detectors that do not disturb the local environments, and crystal scintillation-based gamma detectors are the most suitable sensors for passive long-term measurements.

If there is a priority to make measurements deeper than the shallow surface and monitor radon and other natural gases at a depth of tens of meters, it is necessary to adapt the detector to this configuration.

Finally, all studies based on radon monitoring are confronted with identifying the mechanisms that control radon temporal changes produced within the geological subsurface media. The models that were developed are based on the conventional assumptions that concentration and pressure gradients within the air-filled pores within soil porous media are the main guiding-forces for radon flow by diffusion and advection. For this, a time dependent radon transport equation for the air-filled part of the porous media that combines generation, radioactive decay, diffusion, and advection of radon in porous media, was the best model developed so far (Rogers and Nielson, 1991; Van der Spoel et al., 1998).

This radon transport model for the air-filled part of the porous media as formulated by Van der Spoel (1998) is reproduced below:

$$\beta \frac{\partial Ca}{\partial t} = \nabla \cdot (D \nabla Ca) + \frac{k}{\mu} (\nabla p \cdot \nabla Ca) - \beta \lambda Ca + \Phi$$

β is the partition-corrected porosity, Ca is the radon concentrations in the air-phase (Bq/m³), D is the radon diffusion coefficient in air-filled pores (m²/s), k is the isotropic air-filled permeability (m²), μ is the air-filled dynamic viscosity (kg/m¹s¹), p is the air pressure (Pa) λ is the decay constant of radon (2.1/10⁶ s¹), $\Phi = \lambda \eta p_b C^{Ra}$ is the radon production rate from the immediate parent Ra-226 (Bq/m³s¹), $\nabla \cdot (D \nabla Ca)$ is the diffusive bulk flux density of radon which is proportional to the bulk radon concentration gradient ∇Ca , $\frac{k}{\mu} (\nabla p \cdot \nabla Ca)$ is the radon advective flux density with velocity u , produced by a local gradient in pressure ∇p (deviation from the aerostatic absolute pressure) calculated from Darcy's law: $\nabla p = -\frac{\mu}{k} u$.

But even though the existing model proved to be quite satisfactory for non-isothermal radon transport, it had one major flaw: physical equations do not include temperature, which is one of the most significant parameters affecting gas thermodynamics.

This work builds the experimental basis for extending the above model in order to include explicitly the connection between the temperature gradient and the radon movement.

The data base of the last dozen years will serve to further model radon variability by eventually determining an additional function $F(Ca, \Delta T, \kappa, E_k, T, t)$ to effectively describe and quantify the radon thermal flux from the surface heated by the Sun, to the subsurface porous rock and vice versa. It will allow to determine the gas flux, its direction and range, as a function of: Ca —the concentration of radon in the porous media airspaces, ΔT —the temperature gradient, κ —the thermal conductivity of the gas, E_k —the transitional kinetic energy of the radon atoms as a function of the temperature T ($E_k = 3/2k_B T$), and t —the time.

The Goals of This Work

In this article we intend to summarize the research and achievements, carried out in 7 phases over the past dozen years, in connection with the following subjects:

The radon and CO₂ temporal periodic variability patterns; Differentiating between the effect of atmospheric temperature and pressure on radon and CO₂ flow through a variety of sub terrains media; Eliminating the climatic-induced periodic contributions in order to identify within the measured time series the portion of the signals that could be associated with the regional geodynamic pre-seismic evolution.

The seven stages of work are described below.

Phase I

Response of subsurface Rn-222 to a 20-ton blast experiment investigated at shallow levels during seismic calibration explosion experiment, simulating a 2.6-M_L earthquake, in order to investigate the influence of the explosive blast and the transitory seismic wave fields on the radon transport in the country rock, adjacent to the focus of the explosion (Zafir et al., 2009).

Phase II

The analysis of the temporal behavior of radon and environmental parameters measured continuously at the Amram tunnel, near Eilat (Gulf of Aqaba). The analysis of the results over a period of several years shows radon variability at multiple time scales, associated with the air temperature outside the tunnel, specifically the temperature gradient between the external environment and the more stable environment inside the tunnel (Barbosa et al., 2010).

Phase III

Study of the suitability of silicon photodiodes alpha particles detectors, gamma scintillation sensors and ionization chamber detectors, for utilization in long-term radon monitoring in sub terrain geological media. A comparison of the efficiency and sensitivity, the capability to resolve signal to noise, background, stability, and reliability of their long-term measurements was presented (Zafir et al., 2011).

Phase IV

Long-term high-resolution collection of radon time series carried out in the southern part of Israel. It shows that long-term radon monitoring based on simultaneous alpha and gamma

measurement enables to differentiate between the impact of ambient temperature and pressure on radon transportation within porous media (Zafir et al., 2013).

Phase V

Concurrent radon measurements by gamma and alpha detection systems in a deep drilling hole served as a proxy for studying radon movement within the shallow and deep subsurface, as well as for analyzing the effect of various environmental and tectonic parameters on the radon transport pattern. The technique enabled measuring, for the first time, the radon vertical velocity in the subsurface geologic media as 25 m/hr, and the recovery of a preseismic radon anomalous signal apparently associated with a regional geodynamic process (Zafir et al., 2016).

Phase VI

Open deserted drillings and abandoned wells are an interacting interface between the subsurface hydrosphere, lithosphere, and biosphere to the atmosphere above it. The effect of atmospheric conditions, namely atmospheric pressure and temperature, on air, CO₂, and Rn-222 transport across the borehole-ambient atmosphere interface, was investigated inside a 110 m deep by 1 m diameter borehole in northern Israel. The air exchange rate of these features was analyzed and, consequently their contribution as sources for greenhouse gas (GHG) emissions to the atmosphere was quantified (Levintal et al., 2020).

Phase VII

Long-term monitoring method of Rn-222 and CO₂ at a depth of several tens of meters at Sde-Eliezer site, located within one of the Dead Sea Fault Zone (DSFZ) segments in northern Israel, has led to the discovery of the phenomenon that both gases are affected by underground tectonic activity along the DSFZ, possible related to the pre-seismic processes associated with the accumulation and relaxation of lithospheric stress and strain producing earthquakes (Zafir et al., 2019).

All the technological components used in each of the phases described above included the configuration of a system designed for multi-parametric measurement at a depth of tens of meters, which will be presented in the next section.

EXPERIMENTAL SETTING

Each measurement system installed in the above-mentioned sites included at least two radon gamma detectors and, in some sites, also radon alpha detectors.

Several types of gamma detectors have been adopted: standard (2" diameter) NaI (Tl) gamma scintillation detectors controlled by total count electronic circuit as single channel analyzer (SCA), from two sources—PM-11 system (of Rotem Industries, Israel) and narrow BGO and NaI (Tl) (1.5" diameter) scintillation detectors (of Scionix, Holland).

These BGO and NaI detectors were chosen after we ascertained, depending on the rules listed above, that they have high sensitivity, stability and suitability for use in a 2-inch diameter exploration drilling holes to a depth of several

dozen meters. We have also re-defined the energy range of the SCA used in the Scionix's gamma detectors to count gamma rays only between 475 and 3,000 keV, cancelling the measurement of gamma radiation in the field of the Compton scattering, between 50 and 475 keV, enabling to improve the ratio of signal to noise by 70% in comparison to the PM-11 detection systems (Figure 1A).

The basic principle to choose the SCA for total counting of RDPs gamma rays, is the assumption that radon is the only element within the porous media that can vary in time, under the influence of atmospheric variables or tectonic activity. This fluctuation is observed in addition to the natural gamma radiation from other solid radioactive elements as uranium, thorium and potassium that produce a constant local background (Figure 1B). This validates the use of total counting by gamma detection systems equipped with a SCA for monitoring the temporal variation of radon in geological environment. The sensitivity of Scionix's gamma detectors is 0.01–0.02 Bq/m³ per 1 count/1 hr (see Zafir et al., 2011, based on the comparative test with a calibrated AlphaGUARD detection system, of Saphymo GmbH, Germany).

For radon detection by alpha sensing, the Barasol, BT45 N (Algade Inc., France) is a suitable instrument since it was designed to be used in difficult environments and the calibration of the sensor enables to calculate the volume activity of the Rn-222 in the measured airspace, under undisturbed natural condition. The sensor is an implanted silicon detector with a 400 mm² of sensitive area. It enables the counting of Rn-222 and its daughter alpha products by spectrometry of the alpha particles (with energy between 1.5 and 6 MeV) created in the sensing volume. The sensitivity is about 50 Bq/m³ per 1 pulse/1 hr.

For CO₂ monitoring, the detectors that were lowered down for measurements at depth, were the GMD-20 and GMP-252 infrared gas analyzers of Vaisala, Finland, with measurement ranges of 0–2,000, 0–3,000, and 0–10,000 ppm according to the borehole depth. CO₂ sensor accuracy varied between ±40 ppm with a drift of ±60 ppm/year for the lower range, to ±2% and drift of ±150 ppm/year, for the 0–10,000 ppm range.

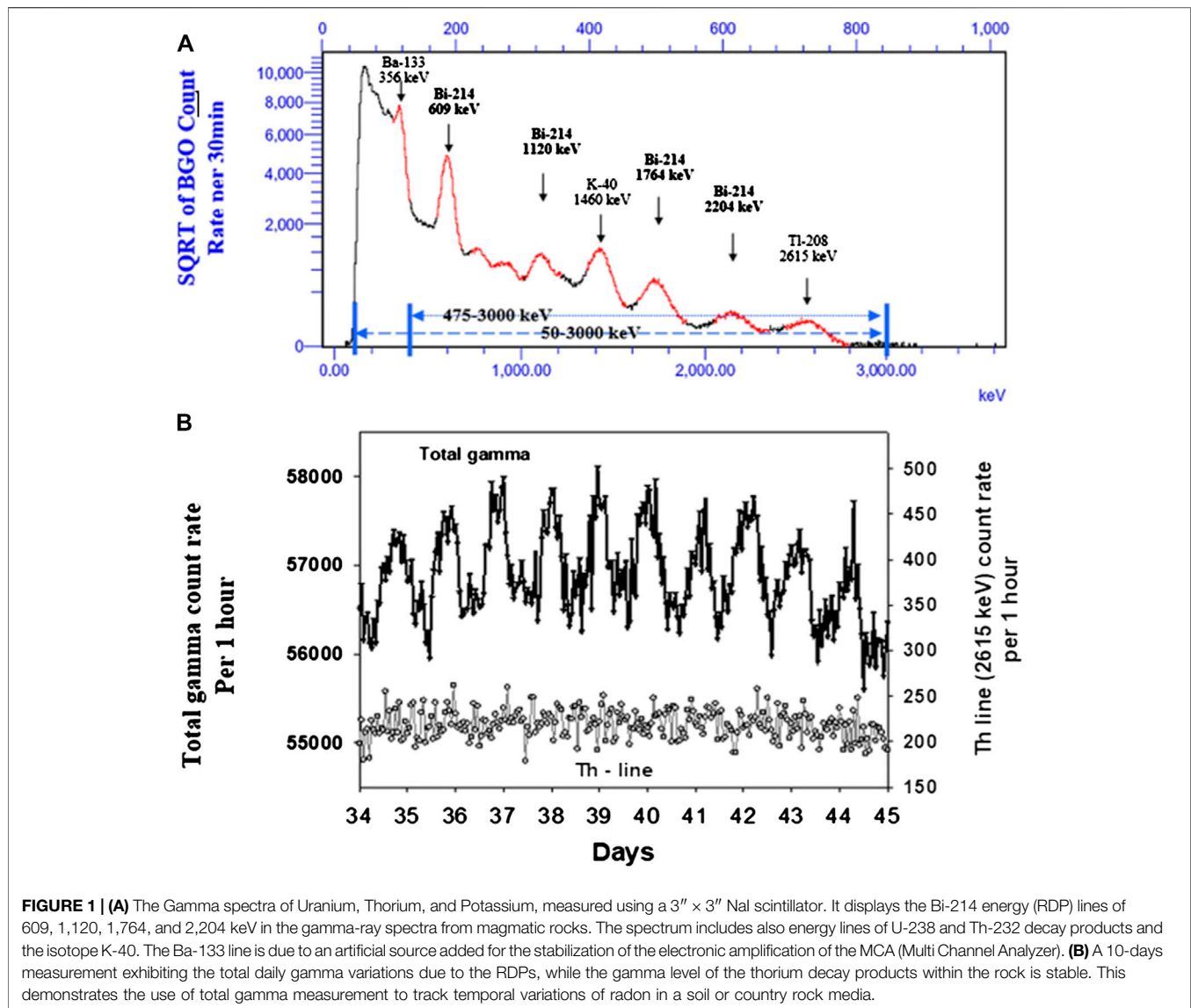
The meteorological variables are measured at each site and with the same high time resolution, as well as complementary parameters such as temperature and relative humidity at depth.

THE RESULTS AND THE ACHIEVEMENTS OF THE CONSECUTIVE STUDIES

Overview

In Israel, the first radon electronic stations were installed in 1995, in the northwestern sector of the Dead Sea. The measurements, with high temporal resolution of 15 min and with adequate sensitivity, showed the presence of a high and temporally fluctuating radon flux in gravel and water (Vulkan et al., 1995).

A research activity based on cooperation between physicists, geophysics, and geologists has begun in Israel, in 2001, aiming to integrate multi-disciplinary scientific methods in Earth sciences



in order to promote the understanding of the processes of earthquake formation and to allow their early prediction (Zafir et al., 2003).

In the last dozen years, about seven combined and diversified studies have been conducted investigating the impact of temperature, pressure, tectonic and other constrains on radon and CO₂ flow within the subsurface geological media, and they are presented in the following sections.

Phase I: Response of Subsurface Rn-222 to a 20-Ton Seismic Calibration Experiment

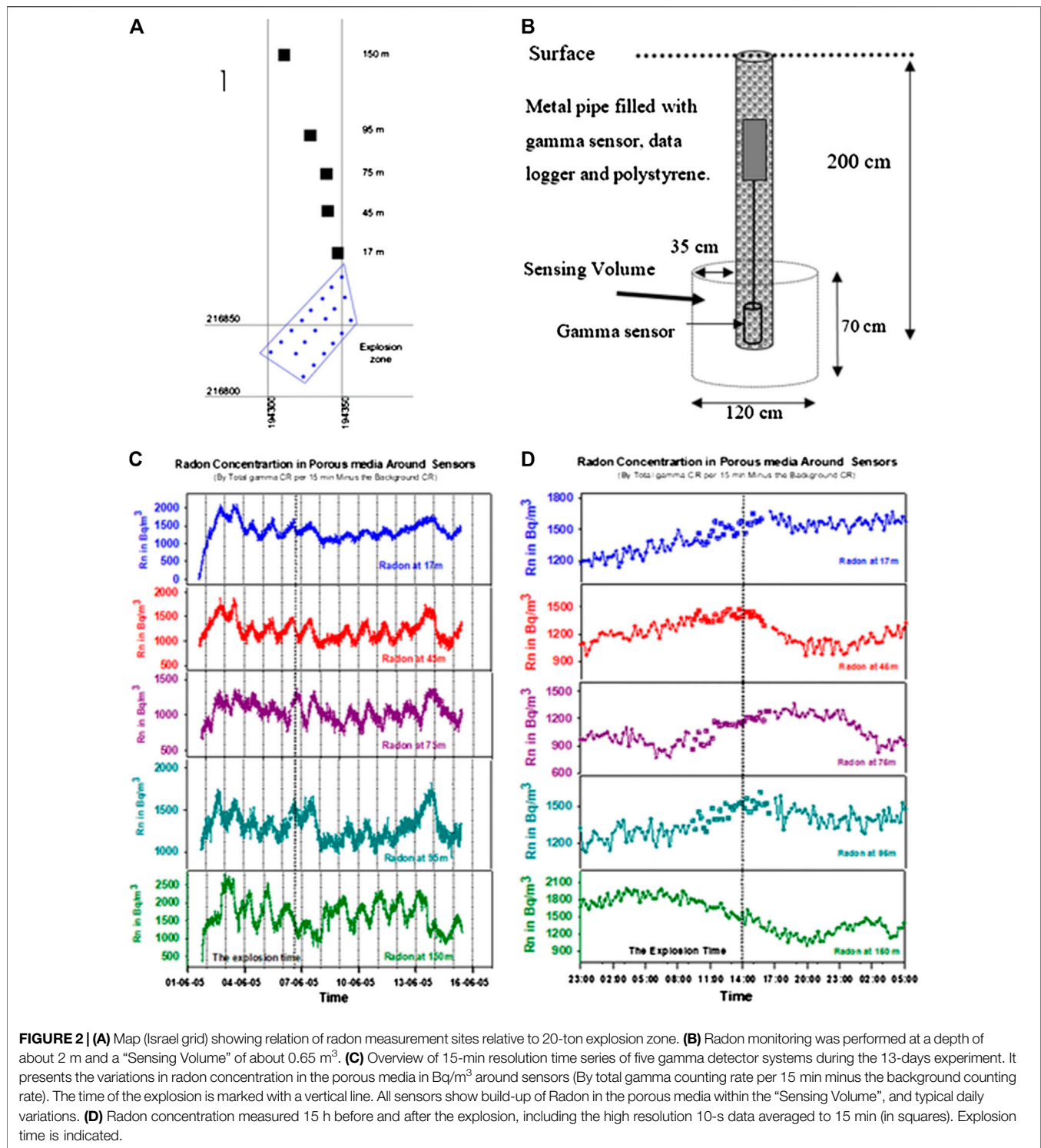
An underground 20-ton explosion for the purpose of performing spatial calibration of a seismic systems array in Israel (Gitterman et al., 2005) was utilized to investigate its effect on the radon movement in the shallow geological media, very close to the focal point of the explosion. A network of five radon detectors was set-up, with the radon sensors installed a few meters apart along

150 m from the center of the explosion. All the detectors were lowered to a depth of 2 m, protected by a metal pipe and suitable cushioning (Figures 2A,B).

Measurements were initiated 4 days before the explosion and carried on for 9 days after the calibration blast with 15 min integration time (Figure 2C). A higher sampling rate of 10 s was inserted in use for few hours before and after the explosion (Figure 2D).

Although it was possible to assume that in the center of the explosion there might be local changes in the radon concentration due to the crushing of the surrounding bedrock, there was no significant change in the radon content along the measuring line of 150 m for the duration of the expansion of the blast wave along this distance, of about 200–400 milliseconds, under acceleration of 1,700 cm/s² (Zafir et al., 2009).

The calculations showed that in this short period of less than half a second, even under a stronger explosion that would create an earthquake simulation even more powerful than the measured



$M = 2.6$, the radon could not respond and move more than 10 cm. Therefore, no changes were measured in the radon concentration at each of the five detectors.

The original article from 2009 includes a calculation showing that around the gamma detector which was close to 17 m from an explosion of 20 tons of explosive material, developed a huge

pressure of about 5 atm that could move radon up to 0.3 m per s. [In comparison to pressure gradient-controlled variations between 10–100 Pa that were sufficient to constrain advective movement within a sand column—Van der Spoel (1998)]. However, the transition time in the explosion that was used for simulating earthquakes with magnitude of 2.6, was 0.25 s.

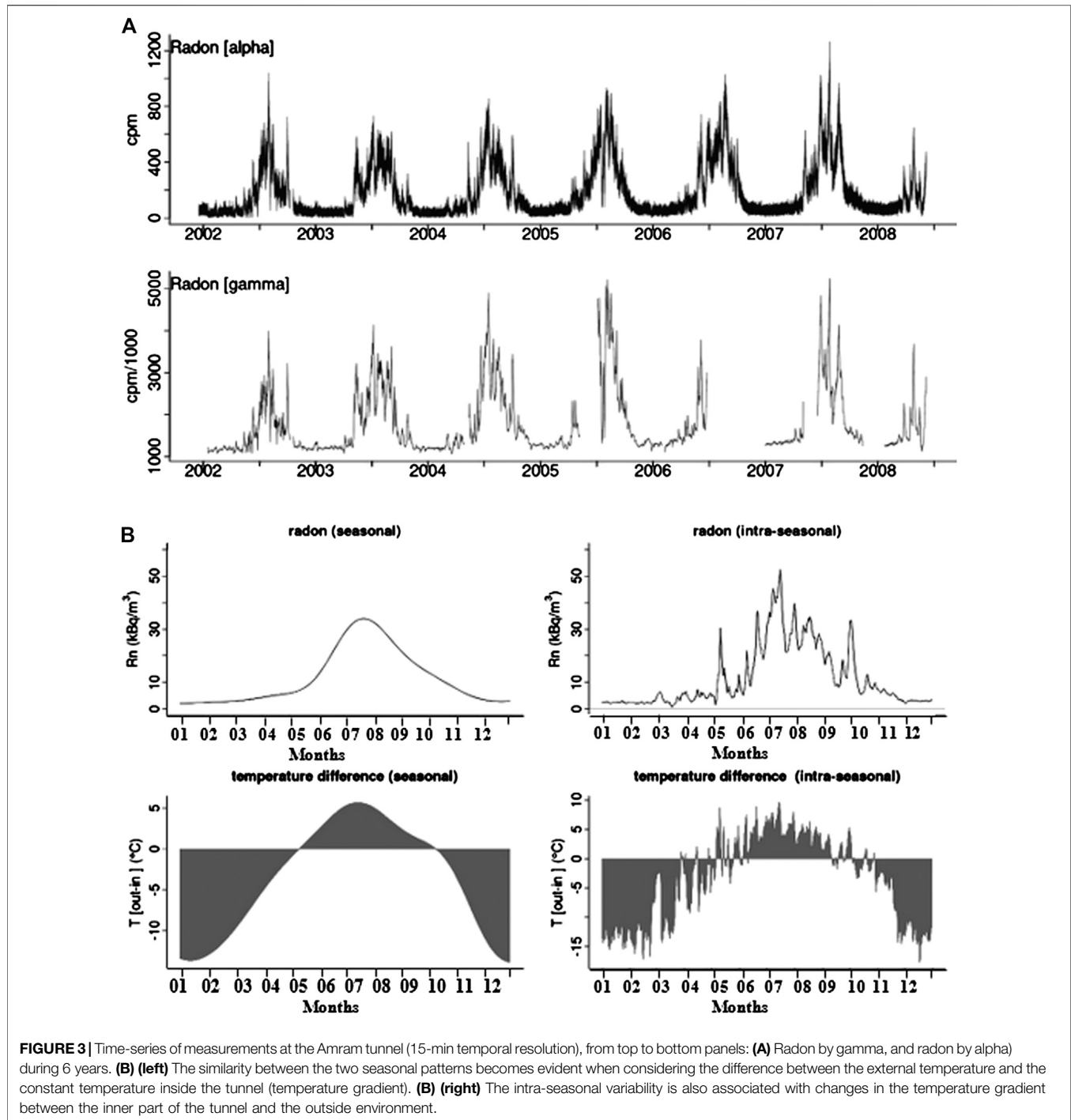


FIGURE 3 | Time-series of measurements at the Amram tunnel (15-min temporal resolution), from top to bottom panels: **(A)** Radon by gamma, and radon by alpha during 6 years. **(B) (left)** The similarity between the two seasonal patterns becomes evident when considering the difference between the external temperature and the constant temperature inside the tunnel (temperature gradient). **(B) (right)** The intra-seasonal variability is also associated with changes in the temperature gradient between the inner part of the tunnel and the outside environment.

Therefore, the time for the pressure impact on the radon gas, even if the EQ energy would be large in some order of magnitude ($M = 4.5$), would still be too short to move the radon gas more than a few meters away.

Hence it is possible to conclude from this experiment that the effect in the subsurface radon concentration of a sudden pressure increase associated with an occurring earthquake is

very reduced, as a result of the very short distance that radon is able to move in such a short time. This does not contradict the possibility of subsurface radon being affected by a pre-seismic event, as the pressure build-up associated with earthquake preparation processes typically develops over much longer time scales, enabling radon movement over larger distances.

Phase II: The Analysis of the Long-Term Temporal Variability of Radon in Research Tunnel

Continuous radon monitoring using co-located alpha and gamma detectors was performed over a period of more than 10 years at the 170 m research tunnel in Mt. Amram. Radon was measured under stable conditions more than 100 m from the tunnel's entrance and below a rock burden of about 100 m (see **Figure 4**, "Phase III: A Comparative Assessment of Radon Sensing Systems for Long-Term Monitoring in Sub Terrain Geological Media" section, **Figure 5**, and "Phase IV: Impact of Atmospheric Aspects on Radon Transportation Within Porous Media" section). This research tunnel in the Arava valley, which is part of the Negev desert, is particularly suitable for the investigation of the factors inducing radon variability, as some of the effects known to influence radon mobility, such as rainfall and soil moisture, are negligible in such a dry (<20 mm/year) environment. The natural environmental conditions in the tunnel are constant, specifically indoor humidity and temperature are kept stable throughout the year. In addition to the radon and environmental parameters which were measured inside the tunnel, air temperature and barometric pressure were also measured outside the tunnel.

The time series resulting from the continuous radon monitoring by both alpha and gamma systems display corresponding temporal variations (**Figure 3A**). Thus, the simultaneous use of alpha and gamma monitoring systems demonstrated that the detailed signals visible in both time series are genuine signals reflecting radon variability, as they are obtained from different detection systems based on distinct measurement principles.

The temporal variability is characterized by a clear seasonal pattern, with maximum values in summer. As expected, the temperature and atmospheric pressure measured outside the tunnel also exhibit a clear seasonal pattern, in contrast the temperature measured inside the tunnel, at a distance of 140 m from the tunnel's entrance, which is very stable along the year with a value of $28 \pm 0.3^\circ\text{C}$. The humidity is also fairly constant and close to 90%.

The temporal variability displayed by the time series of radon and environmental parameters covers multiple time scales, from less than 1 h to years. The decomposition of the time series using the maximal overlap discrete wavelet transform (Percival, 2008) allows to extract the dominant modes of variability and to isolate seasonal, intra-seasonal, and diurnal time scales. The results show that at all the time scales temperature is the main factor responsible for the observed temporal patterns (Barbosa et al., 2010).

At the seasonal scale the variability of radon and temperature is very similar, with both variables displaying a maximum in summer; however, a detailed analysis shows that the temperature outside the tunnel increases since mid-January, while radon concentrations remain low, only increasing slightly in mid-March and then faster by mid-May. However, the similarity between the two seasonal patterns becomes evident when analyzing in detail the difference between the temperature outside the tunnel and the constant temperature inside the

tunnel (hereafter noted as temperature gradient), as displayed in **Figure 3B**, left).

The temporal variability of the temperature gradient also drives intra-seasonal variability. radon anomalies spanning multiple days are only observed when the temperature gradient is positive. This dependence of radon on the temperature gradient is non-linear, as the amplitude of the radon anomaly is not directly related to the amplitude of the temperature gradient, but dependent on the sign of the temperature gradient (**Figure 3B**, right).

As for the case of seasonal and intra-seasonal variability, the daily variations are closely related to the temperature gradient between the internal part of the tunnel and the exterior. Daily variations are absent in the winter, corresponding to a negative temperature gradient. When the external temperature rises and becomes higher than the temperature in the inner part of the tunnel, the radon time series display daily cycles with maximum at night.

Temperature influences natural ventilation as well as radon transport within the porous media. Thus, the mechanisms through which temperature can influence radon variability include temperature-driven air ventilation, through the air medium, and temperature-driven radon migration by thermal gradient dependent function—in the porous media (Nielsen and Bejam, 2006; Zafirir et al., 2007; Zafirir et al., 2008).

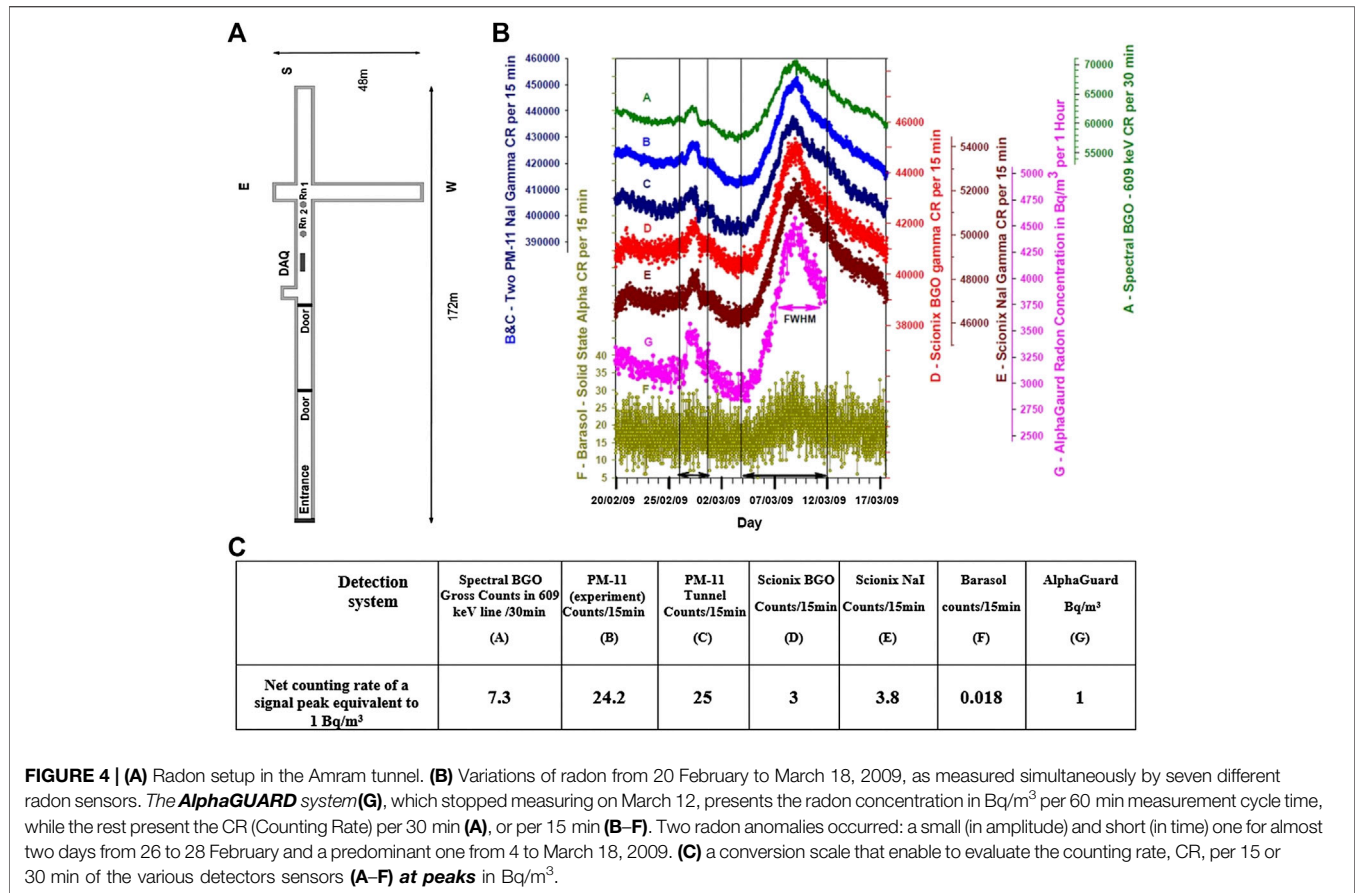
Phase III: A Comparative Assessment of Radon Sensing Systems for Long-Term Monitoring in Sub Terrain Geological Media

A comparative study between alpha particles radon detectors based on silicon photodiode or passive ionization cells, and gamma-rays radon detectors based on scintillation materials, were performed in order to determine their suitability for long-term monitoring in terms of sensitivity, resolution in the parameters of signals intensity and time, as well as long-term operating reliability (Zafirir et al., 2011).

The test system was installed in the research tunnel at Mt. Amram near Eilat, within a closed room at a depth of 140 m (Rn1 and Rn2 in **Figure 4A**). The constant internal temperature of $28 \pm 0.3^\circ\text{C}$ in the tunnel's rooms have enabled the comparison of the various radon detectors under the same environmental conditions. The setup included: Five gamma-ray systems with different dimensions (noted A–E, Rotem, Israel, and Scionix, Holland), one silicon photodiode alpha detector (noted F, Algade, France) and one calibrated ionization chamber (noted G, Saphymo, Germany). All the detectors were exposed over several days to the same natural radioactivity levels under undisturbed thermodynamic equilibrium between the air space and the tunnel walls, recording count rates with high time resolution of every 15 or 30 min (**Figure 4B**).

A conversion scale that enable to evaluate the counting rate (CR) per 15 or 30 min of the various detectors sensors (A–F) at peaks in Bq/m^3 , is included in **Figure 4** (**Figure 4C**).

The main result was that gamma detectors have a high sensitivity between 2 and 4 times in relation to the alpha detectors, enabling the detection of low sub-diurnal radon fluctuations.



In relation to the alpha detector, it was found that the statistical error during the measurements was higher than 20%, because of the low sensitivity (see **Figure 4B**), even in sampling intervals of 30 min [0.022 counts per 1 h for 1 Bq/m³ by the Barasol (F)]. Therefore, in order to identify variations with a required statistical accuracy of at least 5% (which can be obtained easily with each one of the gamma detectors), it is necessary to take measurements with this alpha detector in time periods of at least 8 h or even more.

There is another advantage of using a gamma detector for the measurement of radon temporal fluctuations within the geologic environment: gamma detectors do not violate environmental thermodynamic conditions or the radon secular equilibrium, as happens when grabbing or pumping radon samples. Therefore, the gamma detectors have the highest priority regarding the alternative detectors that were examined in this work. Furthermore, even mechanically it is also harder to handle and lower ionization chambers to typical depths of narrow exploration boreholes.

Phase IV: Impact of Atmospheric Aspects on Radon Transportation Within Porous Media

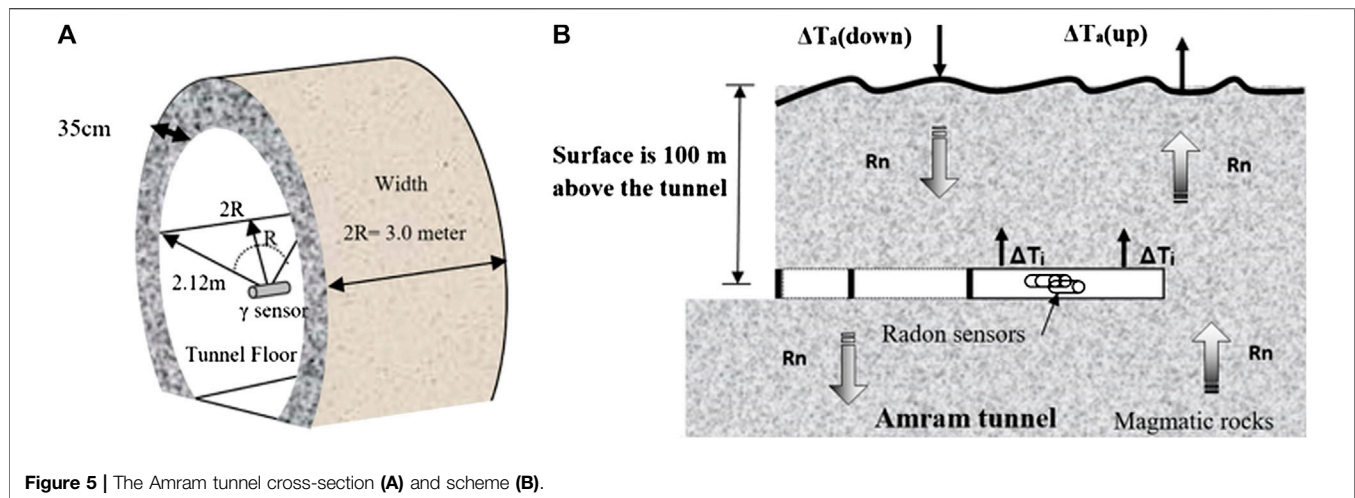
Long-term high-resolution Rn-222 time series, were collected in the subsurface of the southern area of Israel, at the Mt. Amram research tunnel near Eilat and in shallow and deep drillings at

Gevanim site in Makhtesh Ramon (Steinitz and Piatibratova, 2009; Zafir et al., 2013).

In general, if the radon measurements are performed at a tightly closed site, as in the Amram tunnel, the radon within the air space will be in undisturbed environmental conditions and will reach temporal thermodynamic equilibrium with the radon in the bedrocks as well as secular equilibrium with its RDPs, as encountered in the previous “Phase III: A Comparative Assessment of Radon Sensing Systems for Long-Term Monitoring in Sub Terrain Geological Media” section, **Figure 4**.

Then, the radon time series in the tunnel, exhibit daily and seasonal radon levels varying periodically and depending on the climatic temperature gradient outside the rock surface, 100 m above the horizontal tunnel (**Figures 3B, 5B, 6A,B**). The Fourier amplitude spectrum of temperature and of the “summer Radon” is greatly similar (**Figures 6C,E**), and the radon diurnal periodical variations are canceled during the winter (**Figure 6F**).

Hence, the tunnel measurement system reveals a radon signal that pushed down via the country rock porous media, by the daily heating of the surface at a height of 100 m above the tunnel. The heating engine is the gradient temperature ΔT_a (down) pointing downward (**Figure 5B**). In a delay of about 10 h after the maximum exterior heating, the radon signal reaches the tunnel (**Figure 6B**). Ten hours is the time it takes for the gas to flow from the surface to the tunnel. When the surface heating is fading with the external temperature, the size of the temperature gradient ΔT_a is reset and its direction turned upward ΔT_a (up). Then also the radon daily signal fades over time.



In winter, when the temperature inside the tunnel is stable and higher than the surface temperature, the interior temperature gradient ΔT_i is always directed toward the surrounding rock, and inhibits the radon daily flow into the tunnel space (Figures 3B, 5B, 6A).

The temperature gradient is the only geophysical driver available to force the radon via the air-filled space of the surrounding bedrock, as it will be demonstrated also in the next phase (“Phase V: Differentiating Between Radon Anomalies Produced by Climatic Constituent and Pre Seismic Tectonic Activity” section). The alternative mechanism, pressure gradient on the surface, is too weak to compel radon to move along the pore’s media within the bedrock to 100 m depth.

In contrast, the radon concentration in open boreholes in Makhtesh Ramon, as measured in the boreholes air space by the alpha particle’s detectors at 1.2 and 85 m depth, suggests an association with the diurnal (24 h) and semidiurnal (12 h) periodic components and even with multiday barometric pressure variations (Figure 7B). The FFT spectra of the radon signals exhibits a similar component which is different from the temperature periodicity (Figures 7C, 6E).

The appearance of double daily signals like the one circled in drawing 7b is analogous to the pressure’s half-day cycle S2 and S1 (Figure 7C) as presented by Dai and Wang (1999). Those peaks appear locally at 8–10 a.m. and 12–2 night (Steinitz and Piatibratova, 2009), and they demonstrate the connection within the open drilling between the barometric pressure and the radon movement in the inner space (see also “Phase VI: CO₂ and Rn-222 Emissions From an Abandoned Water Well Under the Influence of Climatic Pressure and Temperature” section and “Phase VII: Radon and CO₂ Monitoring Technique in Deep Subsurface, as a Proxy for Investigating Tectonic Pre-seismic Activity” section).

Accordingly, when the semi-daily pressure reaches the minimum (negative pressure in Figure 7B, bottom), the radon can flow into the drilling air space in order to achieve equilibrium. On the other side, when the semi-daily increase in pressure occurs (positive pressure gradient) it prevents the migration of radon from the country rock into the borehole air space. This

mechanism was demonstrated by Van der Spoel (1998), showing that even pressure gradient controlled variations between 10 and 100 Pa were sufficient to constrain advective movement within a sand column.

At the multiday scale, the barometric pressure variations produce a long multi-day radon signals at a borehole depth of 85 m, with the same time span as in the shallow depth of 1.2 m (Figure 7B, top). But the radon daily and half a day periodicity that was observed at 1.2 m air space is concealed at the depth of 85 m most of the time except for few days when the pressure varies around 950 mbar level.

The understandings and knowledge that came out of this study, about utilizing in parallel two different types of radon measurement methods in closed and open-air spaces, led to the idea to operate these combined methods of radon measurement within deep abandoned boreholes as a proxy for underground geodynamic research.

Phase V: Differentiating Between Radon Anomalies Produced by Climatic Constituent and Pre Seismic Tectonic Activity

The combination of long-term, radon measurement by gamma and alpha methods within deep abandoned boreholes enabled to distinguish between radon anomalous signals at depth induced by the periodical climatic parameters (temperature and barometric pressure), and those that may be driven by deep tectonic processes along active seismic faults. The concurrent identification of radon signals in various depths with 50 m between them, allowed for the first time to calculate the radon vertical velocity in the bedrock under the influence of the temperature gradient on the surface. It also revealed a radon anomaly that apparently occurred ahead of a tectonic event, the Nuweiba earthquake, which occurred within the Dead Sea Fault Zone on June 27, 2015, with magnitude of $M = 5.5$ (Zafir et al., 2016).

The first deep dedicated combined radon monitoring system was installed in January 2015 at an abandoned water well (110 m

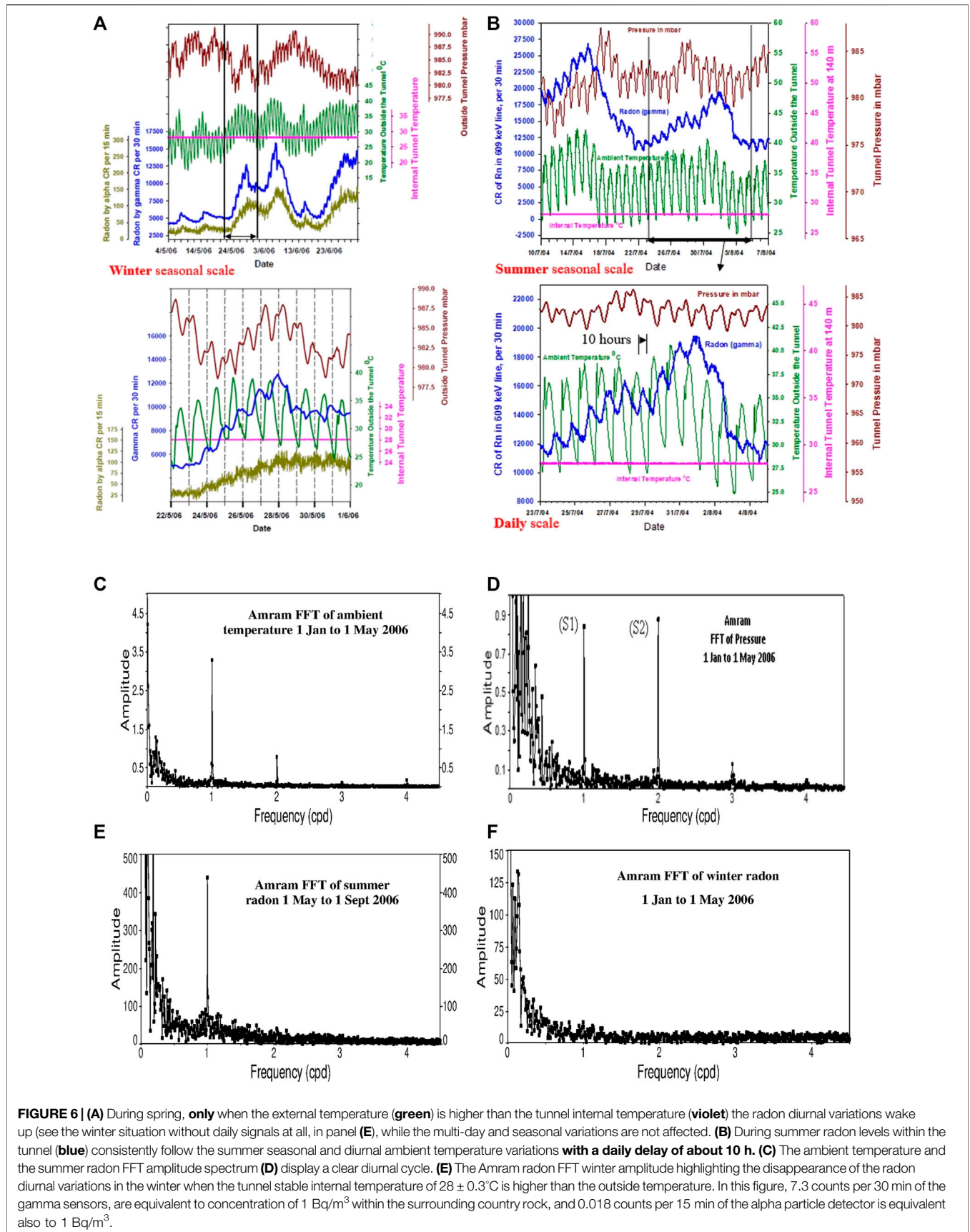
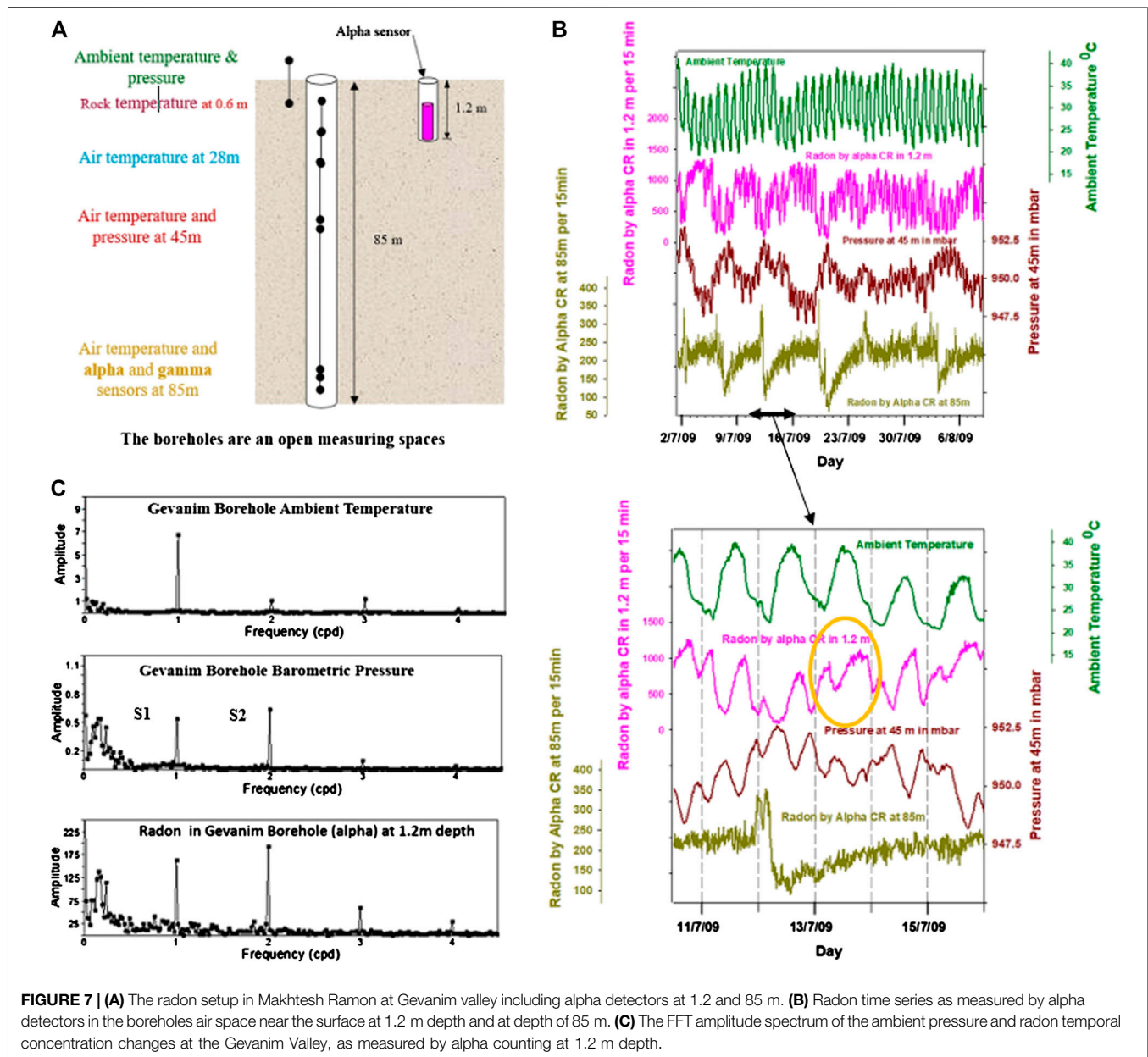


FIGURE 6 | (A) During spring, **only** when the external temperature (green) is higher than the tunnel internal temperature (violet) the radon diurnal variations wake up (see the winter situation without daily signals at all, in panel (E)), while the multi-day and seasonal variations are not affected. **(B)** During summer radon levels within the tunnel (blue) consistently follow the summer seasonal and diurnal ambient temperature variations **with a daily delay of about 10 h**. **(C)** The ambient temperature and the summer radon FFT amplitude spectrum **(D)** display a clear diurnal cycle. **(E)** The Amram radon FFT winter amplitude highlighting the disappearance of the radon diurnal variations in the winter when the tunnel stable internal temperature of $28 \pm 0.3^\circ\text{C}$ is higher than the outside temperature. In this figure, 7.3 counts per 30 min of the gamma sensors, are equivalent to concentration of 1 Bq/m^3 within the surrounding country rock, and 0.018 counts per 15 min of the alpha particle detector is equivalent also to 1 Bq/m^3 .

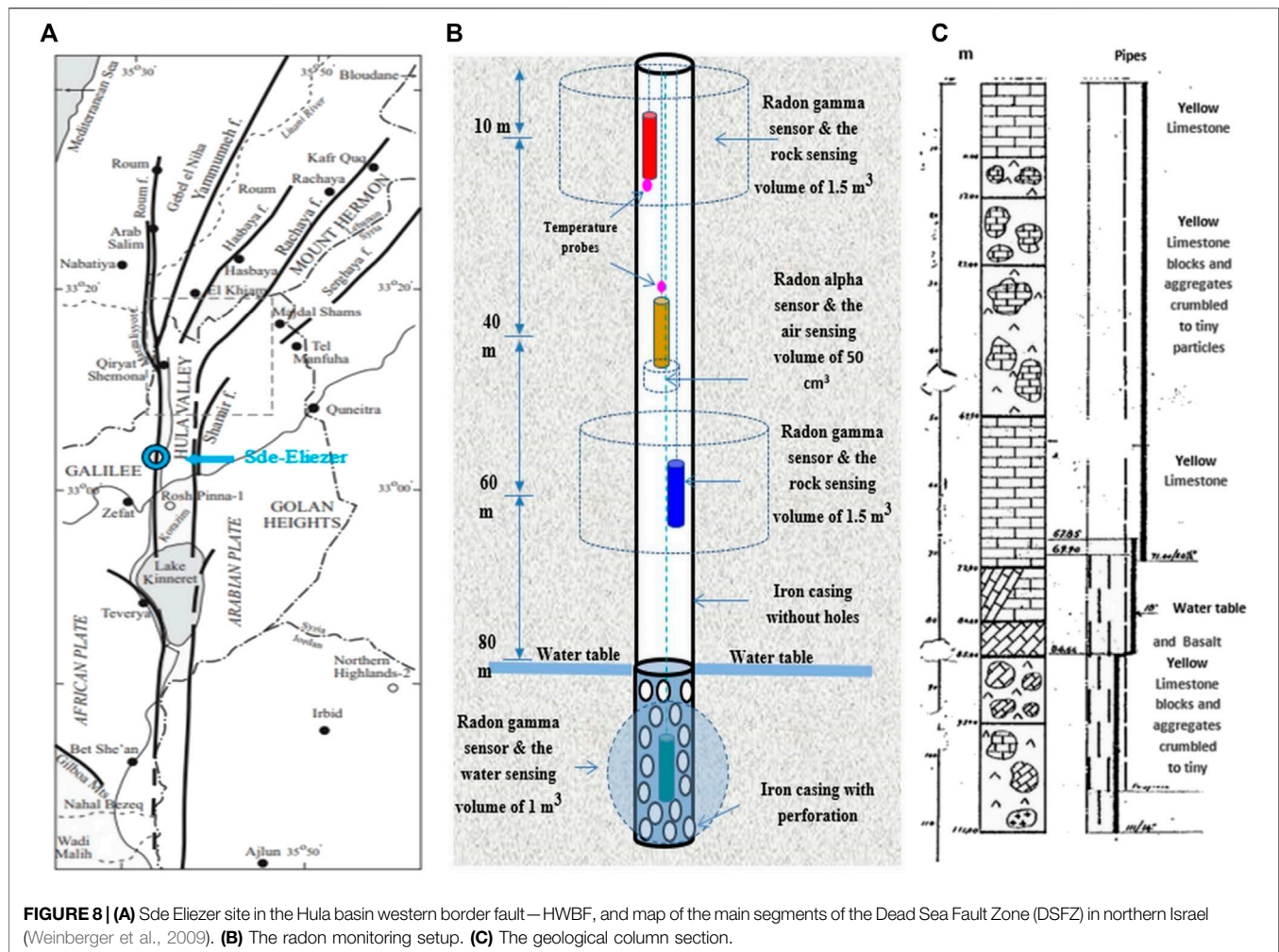


depth and about 1 m diameter) at the Sde Eliezer site, which is located within the Hula Valley western border fault (Figure 8A).

Lowering simultaneously gamma and alpha radon detectors to different depths within the deep borehole (Figure 8B) and monitoring their temporal variations, enabled to differentiate in the radon time series signals, between the daily periodical influence of the ambient temperature (stars in Figure 9A) and the semi-daily effects of the barometric pressure (arrows in Figure 9A).

The gamma detectors at 10 and 60 m depth at Sde-Eliezer site (Figures 8B, 9A,B) are narrow BGO detectors, presented in “Experimental Setting” section and “Phase III: A Comparative Assessment of Radon Sensing Systems for Long-Term Monitoring in Sub Terrain Geological Media” section. These detectors measure contributions from a source volume of 1.5 m³ of surrounding bed rock (Figure 8B).

According to Figure 9A the maximum signal in the raw data for the BGO gamma sensor at the depth of 60 m (for example, in blue in 27/4/15), is about 53,000 counts per 15 min minus the background of 4,000 counts per 15 min. It is thus equal to a net rate of 49,000 counts per 15 min, which is equivalent to 16,333 Bq/m³ according to the above calibration scale (Figure 4c). This peak is reached, with a delay of about 2 h from the peak of the radon in the borehole airspace, as measured by the alpha sensor at 40 m (see Figure 9C). This radon peak of 125 counts per 15 min, with a background of five counts, corresponds, according to the stated calibration scale (Barasol sensor) to $120/0.018 = 6,666 \text{ Bq/m}^3$. This fact proves that the concentration of the radon within the sealed iron casing airspace (see Figure 8B) corresponds to less than 40% of the radon content that is measured by the gamma detector.

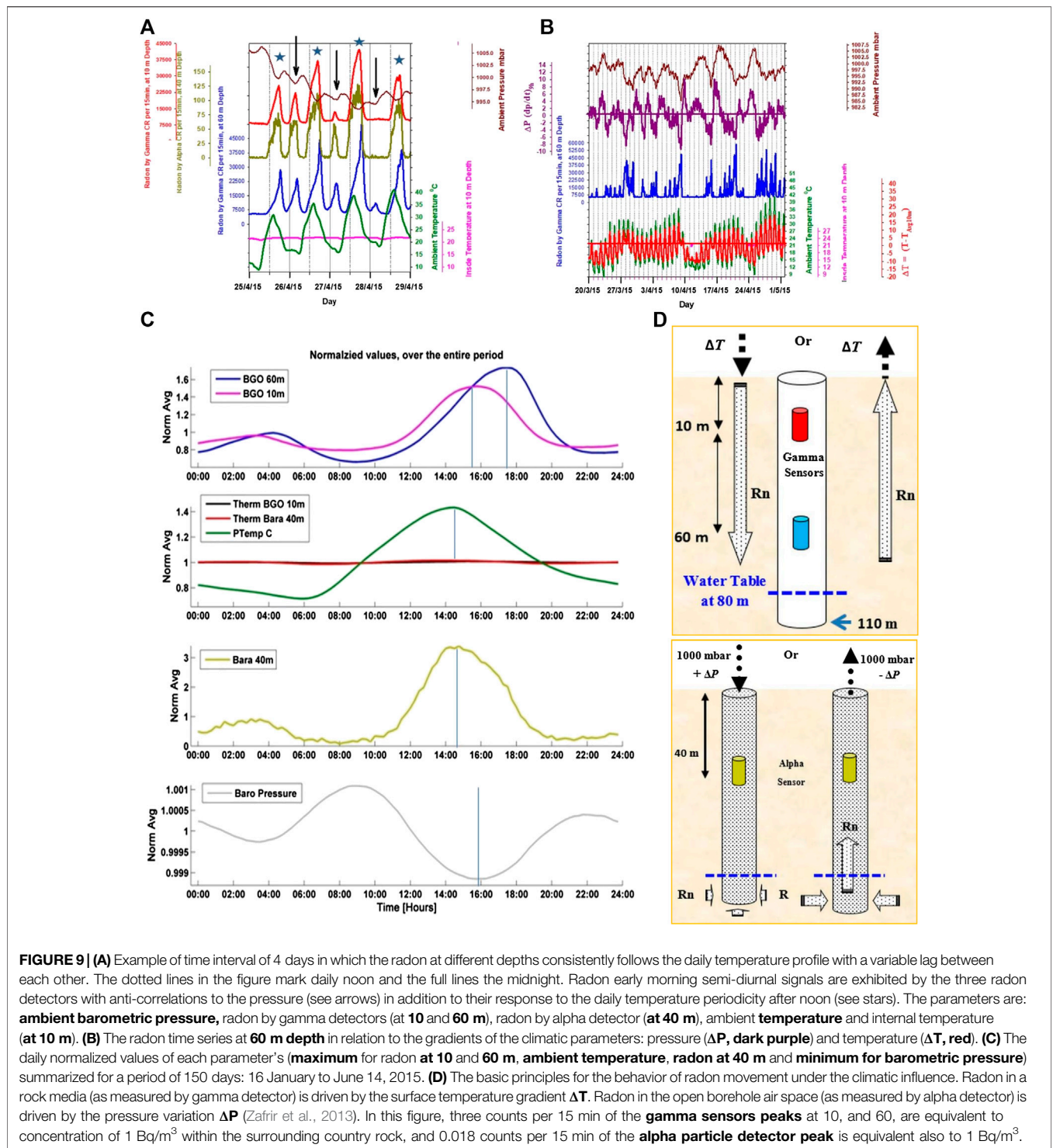


Thus more than half of the gamma counts result from the contribution of the radon in the surrounding bedrock in the form of a background from the radon that remains stuck within the rock grains, and a variable part from the radon able to move within the rock porous media, mainly driven by the influence of the Sun heating on the surface creating a temperature gradient (“Phase II: The Analysis of the Long-Term Temporal variability of Radon in Research Tunnel” section, and “Phase IV: Impact of Atmospheric Aspects on Radon Transportation Within Porous Media” section). The background portion is a further proof that this contribution originates from outside the iron pipe, as it does not decrease to near zero as the radon signal within the casing airspace does under the effect of the positive barometric pressure gradient (Figures 9B,C).

The semi-daily cycle measured by the gamma and alpha detectors (Figure 9A) results from the radon which is pumped from the water into the well airspace by the barometric extraction (minima) at early morning, as measured by the alpha detector at 40 m. The secondary peak of the three radon signals appear at around the same hour, 4 a.m. (Figure 9C). The contribution from the mobile radon within the surrounding bedrock to the radiation measured by the gamma detectors is very low at that time.

In addition, the pronounced time delays between the radon peaks measured by the three sensors (Figure 9C), prove that if all the radon variations would happen in the same borehole airspace then we would have to look for fast streaming from the middle (the first peak at 40 m) upward to 10 m and then back downwards to reach the 60 m level 2 h later. It seems very unlikely as there is a single direction of CO₂ streaming, from 70 m level to 40, 20, and 5 m, and vice versa, as described in “Phase VI: CO₂ and Rn-222 Emissions From an Abandoned Water Well Under the Influence of Climatic Pressure and Temperature” section and in Figures 10B,D, with a faster air velocity between 2 and 6 m/min (120–360 m/h).

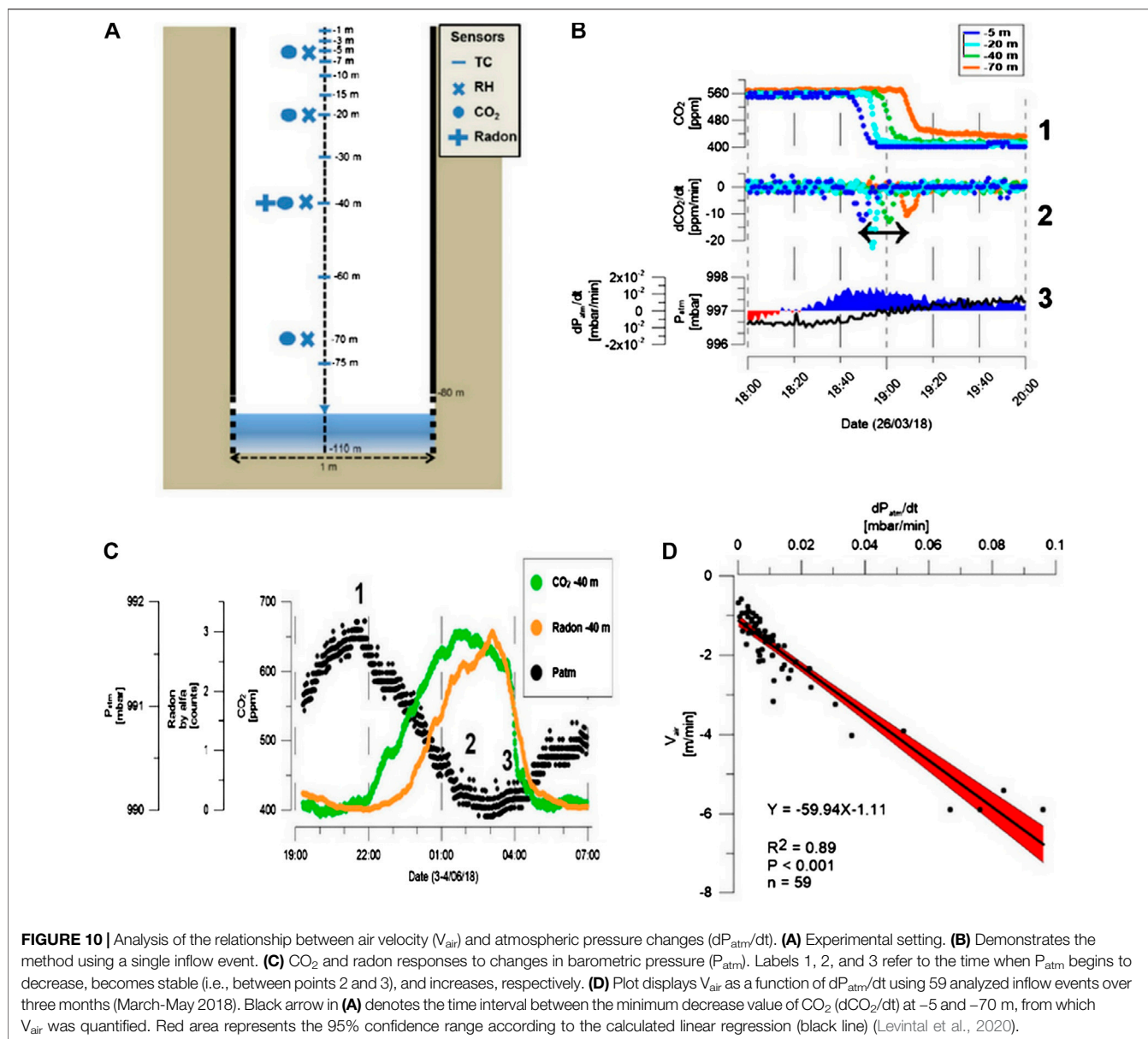
Now, considering the radon temporal variation in the bedrock around the pipe. From 10 m downward, we would find after about 2 h a similar concentration peak of about several thousand Bq/m³ at a depth of 60 m, high above the radon concentration within the borehole airspace that reduced at that moment to at least half level (Figure 9C). The temperature-driven downward movement of radon outside the sealed casing, brings radon into the saturation zone at 80 m. Since the borehole casing is not perforated down to the water table, radon can only enter the casing from the groundwater. Considering that Ra-226 was not found in the



Sde Eliezer water, radon streamed downward into the groundwater via the porous rock, driven down by the surface temperature gradient ΔT . It means that the groundwater is the source for supplying radon to the open borehole air space.

In a shallow, open, abandoned wells such as the Sde-Eliezer well, long-term equilibrium between the radon within the porous

media and inside the open borehole air space is not necessarily established. Therefore, the radon measured by the gamma and the alpha detectors is different. The negative barometric pressure gradient is the driving force that pumps the radon upward via the open borehole (as named Barometric Pumping in “Phase VI: CO₂ and Rn-222 Emissions From an Abandoned Water Well Under the Influence of Climatic Pressure and Temperature” section).

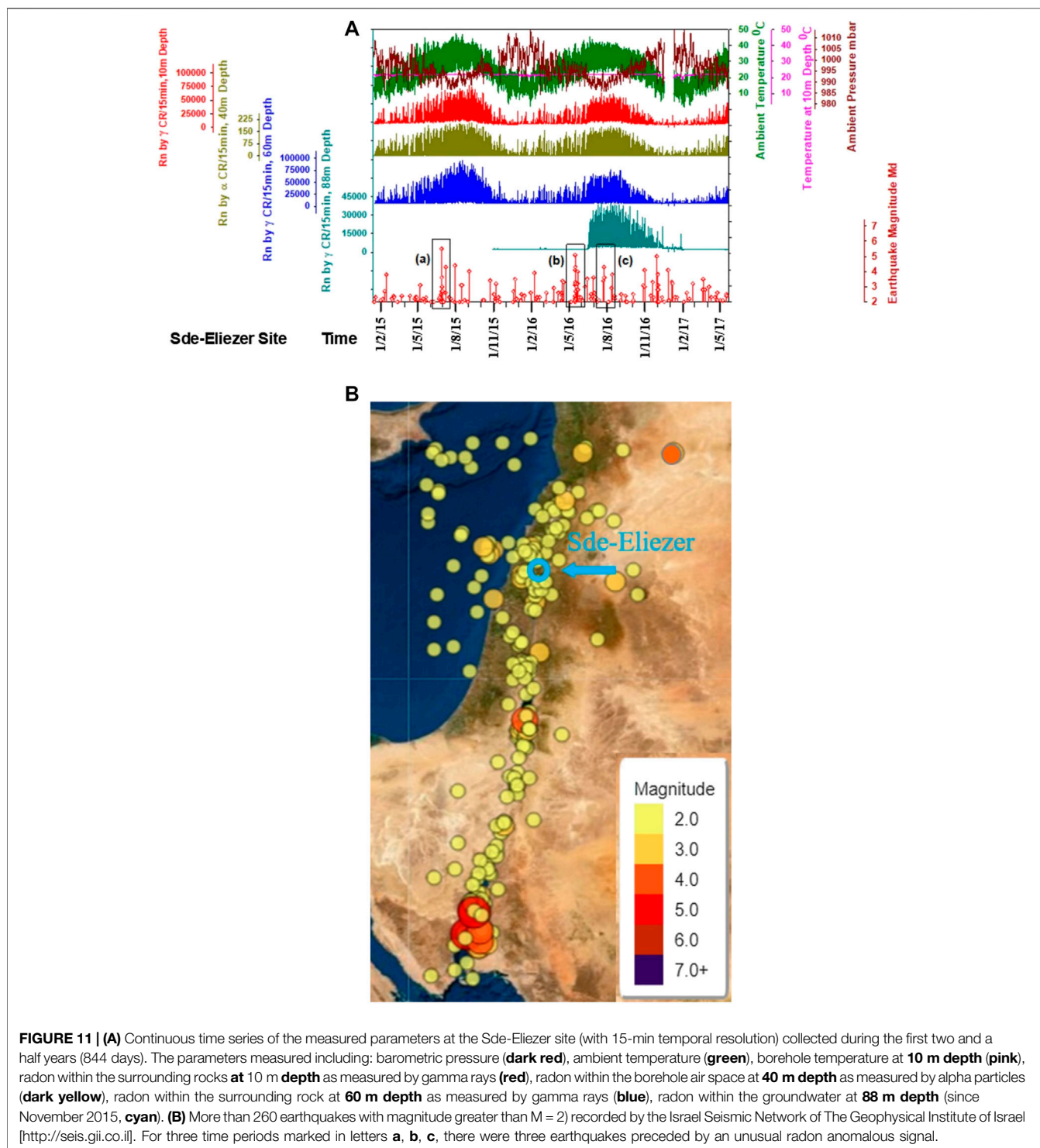


The assumption that radon can flow downward via the porous media is also suggested from other measurements at diverse sites, including various time delay measurements (see “Discrimination Between the Influence of Climatic Temperature and Pressure on Radon Flow in Geological Media” section).

Analyzing the time series in detail, (Figure 9B) an interesting relationship between the radon signals and the gradients of both temperature and pressure parameters appears: the disappearance of the radon signals at some time intervals, as occurred on 22 March, 30 March, 10–14 April, or 23–24 April. This phenomenon is related to the inversion of the temperature gradient $\Delta T = T - T_{10m}$, from positive to negative (when T_{10m} is the stable temperature in the well at a 10 m depth). This situation happens when the outside

temperature becomes lower than the constant temperature of 21.29°C at the 10 m depth (as described in “Phase II: The Analysis of the Long-Term Temporal variability of Radon in Research Tunnel” section and “Phase IV: Impact of Atmospheric Aspects on Radon Transportation Within Porous Media” section). It is also happened when the inversion from negative to positive occurred of the pressure gradient $\Delta P = dP/dt_{9h}$, from negative to positive occurred, leading to the same effect. The disappearance of radon daily signals because of the inversion in the temperature gradient was already observed (Barbosa et al., 2010; Choubey et al., 2011).

The whole process is very clear: the higher the external temperature, the more gas will flow down the bedrock. If more radon gas reaches the water, then more radon is sucked into the well airspace. At noon, because parallel to the rising of the



external temperature during the day, the barometric pressure is decreasing accordingly, and the barometric pumping is getting stronger. Then, more radon is measured by the alpha detectors at a depth of 40 m (**Figure 9A**).

The time lag of about 2 h between the maximum values of the two gamma detectors separated vertically by 50 m, defines the

radon vertical velocity as 25 m/h in the local subsurface porous media (**Figure 9C**). This is the first determination of the downward radon transportation velocity within porous rock media, by direct field measurement. It also proves that radon in the Amram tunnel moves downwards to the tunnel (100 m depth) in 10 h (**Figure 6B**).

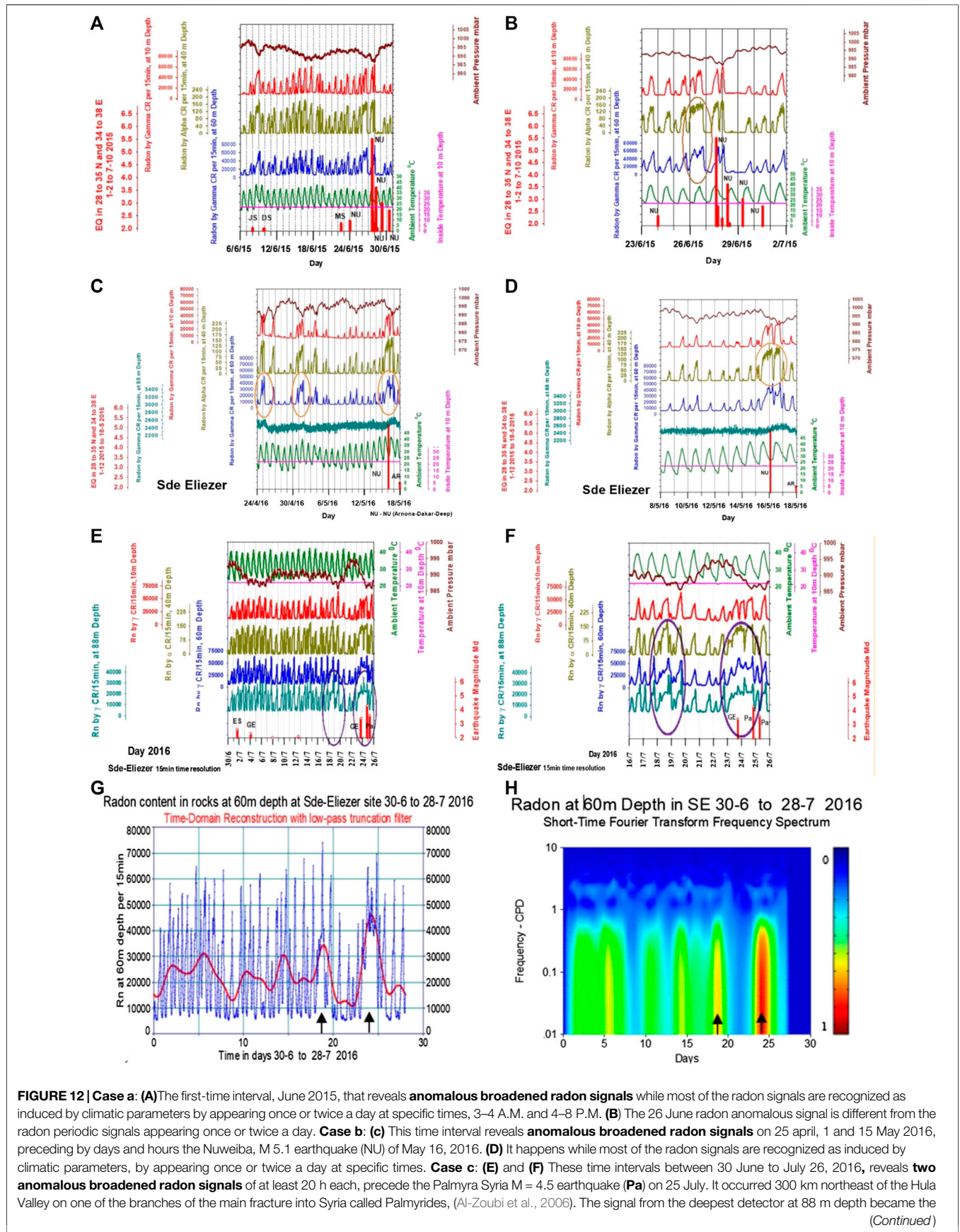


FIGURE 12 | Case a: (A) The first-time interval, June 2015, that reveals **anomalous broadened radon signals** while most of the radon signals are recognized as induced by climatic parameters by appearing once or twice a day at specific times, 3–4 A.M. and 4–8 P.M. **(B)** The 26 June radon anomalous signal is different from the radon periodic signals appearing once or twice a day. **Case b: (c)** This time interval reveals **anomalous broadened radon signals** on 25 April, 1 and 15 May 2016, preceding by days and hours the Nuweiba, M 5.1 earthquake (NU) of May 16, 2016. **(D)** It happens while most of the radon signals are recognized as induced by climatic parameters, by appearing once or twice a day at specific times. **Case c: (E)** and **(F)** These time intervals between 30 June to July 26, 2016, reveals **two anomalous broadened radon signals** of at least 20 h each, precede the Palmyra Syria M = 4.5 earthquake (Pa) on 25 July. It occurred 300 km northeast of the Hula Valley on one of the branches of the main fracture into Syria called Palmyrides, (Al-Zoubi et al., 2006). The signal from the deepest detector at 88 m depth became the *(Continued)*

FIGURE 12 | most pronounced since the water table within the borehole of the abundant well, dropped down below 100 m, **by unique event** on June 25, 2016 (see **Figure 11**) as a result of massive pumping in the Hula Valley area, since February 2016, because of a drought. The EQs locations are Palmyra (**Pa**), Gulf of Eilat (**GE**) and East Sinai (**ES**). (**G**) and (**H**) are the FFT low-pass filtering and the reconstruction spectrogram of the radon's 60 m time series in the time interval of 30 June to July 27, 2016, shows the **discrete radon broadened signals** that are marked in the with **black arrows**. The results of the FFT filtering and the time domain reconstruction of the above time intervals (**E**) show that although the procedure does not disable the entire cyclical signature in the original data, it keeps the **seasonal fluctuated background** under 30,000 counts per 15 min at the 60 m radon gamma detector. (**H**) The reconstruction STFT spectrogram of the radon 60 m time series in the same time interval. **The procedure pinpoints the two broadened signals 6 and 2 days before the earthquake on July 25, 2016.** The FFT analysis have done to each one of the above cases. In this figure, three counts per 15 min of the gamma sensors at 10, 60 and 88 m, are equivalent to concentration of 1 Bq/m³ within the surrounding country rock, and 0.018 counts per 15 min of the alpha particle detector is equivalent also to 1 Bq/m³.

The most important observation in the study of the radon time series obtained during the first 10 months of 2015 at the Sde Eliezer site, was the discovery of a broadened pre-seismic radon signal (wider than the sum of the expected width of the diurnal and semidiurnal radon signals combined) that have been ahead by one day (**Figure 12** at “Phase VII: Radon and CO₂ Monitoring Technique in Deep Subsurface, as a Proxy for Investigating Tectonic Pre-seismic Activity” section) the Nuweiba M = 5.5, 4 km deep earthquake, which happened on June 27, 2015, near Eilat (GE) about 480 km from Sde-Eliezer site at Hula Valley. It was the first evidence that a pre-seismic earth strain, stress or deformation along an active fault like the DSFZ, may produce a faraway local pressure gradient (Aharonov and Scholtz 2018) to induce, non-periodic, radon anomalies.

Since no experimental method proved or contradicted, the assumption that a long-lasting stress or strain produced during pre-seismic rupture processes can exist and operate along active faults, far away to hundreds of kilometers, we can raise the hypothesis that a pressure gradient in the magnitude of a few pascal (10⁻⁵ atm) can be produced by pre-seismic tectonic driving forces in the subsurface, and induce radon and CO₂ anomalous flow within the porous media, even for strains below the tidal magnitude of ~10⁻⁸. Models to assess the total strain that can develop in geological media before seismic events, to a distance of a few hundred kilometers from the center of the earthquake, as a function of its magnitude, were presented in the literature (Cicerone et al., 2009; Wang and Manga, 2010; Skelton et al., 2015; Woith et al., 2018).

Phase VI: CO₂ and Rn-222 Emissions From an Abandoned Water Well Under the Influence of Climatic Pressure and Temperature

Boreholes and wells are a complex interplaying interface between the subsurface hydrosphere, lithosphere, and biosphere to the atmosphere above it. Quantitative computing the air exchange rate between these features is therefore very relevant, as these are potential sources for greenhouse gas (GHG) emissions to the atmosphere. The influence of atmospheric conditions, including barometric pressure and ambient temperature, on the air, CO₂, and radon transport across the borehole-ambient atmosphere interface and groundwater-borehole bottom interface is studied based on measurements inside a 110 m deep by 1 m diameter borehole in Sde-Eliezer site in northern Israel (Levintal et al., 2020).

For CO₂ monitoring, the detectors that were lowered down to acquired measurements at depths of 5, 20, 40 and 70 m, were the GMD-20 and GMP-252, infrared CO₂ analyzers (Vaisala, Finland), with measurement ranges of 0–2,000, 0–3,000, and 0–10,000 ppm conforming to the borehole depth.

In parallel the setup included thermocouples (T type) and Relative Humidity probes (Humitter ⁵⁰U, also of Vaisala, Finland) at almost the same depths, and radon alpha-particle detector (Barasol of Algade Inc., France) as described previously (“Experimental setting” section, “Phase III: A Comparative Assessment of Radon Sensing Systems for Long-Term Monitoring in Sub Terrain Geological Media” section, and “Phase IV: Impact of Atmospheric Aspects on Radon Transportation Within Porous Media” section).

- The high resolution of CO₂ measurements enables to determine *in-situ* the air velocities within the borehole. During barometric pumping (BP), when there is inflow of atmospheric air from the top to the bottom direction, the CO₂ measured by the upper sensor (–5 m) is expected to decrease before the CO₂ variation will be measured at the bottom (–70 m). Then the distance of 65 m between the two sensors can be divided by the time interval between sensor responses, in order to get the vertical component of the CO₂ velocity within the borehole (Vair), assuming that CO₂ transport is advective—carried as part of the air mass movement within the borehole. The basic assumption was based on the photographed proof that the borehole casing above the 80 m depth is a sealed iron pipe, and the only CO₂ inlet and outlet are the bottom or the top entries. Therefore, the minimum value of dCO₂/dt provides an easily identifiable signal. The time difference between sensors' minimum value used to calculate the velocity of the atmospheric air pulse between sensors. This analysis is illustrated in **Figures 10B–D**. Preliminary calculations indicated that the average vertical CO₂ velocity inside the borehole equal ~1.3 m/s.

Calculating the air exchange rate at the well from the measured air/CO₂ velocities, using two independent methods as detailed in Levintal et al., 2020, (fluctuating up to ~6 m/min) gave a mass flux rate to the atmosphere of ~5 g-CO₂/min CO₂ emissions, becoming higher during the summer with two daily peaks as presented for example in **Figure 15** at the next “Phase VII: Radon and CO₂ Monitoring Technique in Deep Subsurface, as a Proxy for Investigating Tectonic Pre-seismic Activity” section.

This reveals the time-dependent behavior of boreholes as an additional source of CO₂ emissions. On a yearly scale, the calculated CO₂ emissions from Sde-Eliezer site were similar in magnitude to a wheat field in the range of 100 to 6,000 m².

The most notable results are summarized as follow:

- Barometric pressure changes were the governing mechanism for air movement along the well. The thermal internal instability played a minor role.
- CO₂, water vapor, and radon, moved along the air space in a similar manner.
- The transport of gases from the vadose zone to the atmosphere via the borehole airspace depends on two processes: the transport of the pore gas into the borehole lower entry, and the movement of the gas out of the borehole and into the atmosphere.

Phase VII: Radon and CO₂ Monitoring Technique in Deep Subsurface, as a Proxy for Investigating Tectonic Pre-seismic Activity Overview

Long-term monitoring method of Rn-222 and CO₂ at a depth of several tens of meters at Sde-Eliezer site, located within one of the DSFZ segments in northern Israel (Phase V: Differentiating Between Radon Anomalies Produced by Climatic Constituent and Pre Seismic Tectonic Activity), has led to the discovery of the phenomenon that both gases are affected by underground tectonic activity along the DSFZ, possible related to the pre-seismic processes associated with the accumulation and relaxation of lithospheric stress and strain producing earthquakes (Zafir et al., 2019).

The Results of the First Period From February 2015 to May 2017

The first period of the long-term radon monitoring carried out at the Sde-Eliezer site lasted for two and a half years (844 days) from February 2015 to May 2017. In parallel, about 260 earthquakes with magnitude $M \geq 2.0$, that have been recorded during the 844 days along the DSFZ area, was added to the acquired data (**Figure 11A**). The DSFZ area in **Figure 11B** is defined by the Geophysical Survey of Israel as the region from 27° to 36 N in latitude and longitude from 32° to 38 E (see <https://earthquake.co.il/en/earthquake/searchEQS.php>).

The largest variations in the radon temporal flux are mostly controlled by the temperature gradient on the surface as can be observed in **Figure 11A** at different depths.

The role of the temperature gradient on radon temporal behavior is probably not linear since the ratio between the radon level in winter to summer varies by a factor of 3–10 (**Figure 11A**), while the temperature varies within 10% span (28° change vs. 285K). In parallel, the pressure effects, according to the existing physical model, arise linearly through the negative pressure gradient term. Therefore, it is impossible to predict so far, the total impact of the temperature and pressure at particular time, by the current contemporary model.

Other climatic variables, such as rain and snow, were found unimportant according to the results between winter and spring (December to end of March) and the long Israeli summer (April to November) during which there are no visible signs of rain or snow.

In addition, three, very pronounced radon signals that were different in shape and preceded earthquakes with magnitude >4.5 , appeared during disparate events which occurred during the above-mentioned two-and-a-half-year, and marked by **a**, **b** and **c** in **Figure 11A** as presented in the following section.

The Data Analysis Methods to Identify the Nature of the Gases Anomalies

The procedure to exclude periodical radon signals.

Since the existing radon model and the physical equations for radon transport in the subsurface geologic media do not include temperature, which is one of the most significant parameters affecting gas thermodynamics, it is difficult to predict the radon temporal behavior induced by this parameter as was done for the barometric pressure (Perrier and Girault, 2013). On the other hand, in order to identify the nature of the residual anomalies, their specific contribution must be excluded from the measured time series.

One of the possible methods for isolating the components belonging to the periodic signals produced by the climatic parameters in the measured time series is to apply the Fourier domain filtering and component isolation procedure (AutoSignal™, Systat Software Inc.).

Utilizing these existing algorithms that work in the frequency domain for low pass truncation, frequency components above a chosen ideal cutoff frequency be removed from the original radon time series, leaving the frequencies below it unaltered as well as any non-periodic discrete events.

Choosing a frequency cutoff less the diurnal one (1 cycle per day) excludes all the unwanted diurnal, semi diurnal and higher periodical signals (maybe harmonics) that are induced by the atmospheric parameters.

Another extraction method that relies on the Modulation Spectral Analysis is the spectrogram phase space representation in which one may see simultaneously the temporal as well as the spectral information of a given signal.

The main advantage of using a spectrogram is its capability of being a better visualization tool showing in a more emphasized manner the relevant temporal anomaly.

In any case, we have proved by the two methods, based on FFT low-pass truncation filtering and the time domain reconstruction analysis, that indeed a radon anomaly is identified and that it lasts for more than 20 h.

The Recovery of a Pre-seismic Radon Anomalous Signal Apparently Associated With a Regional Geodynamic Process

These are the three disparate events that occurred during the above-mentioned two-and-a-half-year, in which very pronounced radon signals seem to preceded earthquakes with magnitude >4.5 :

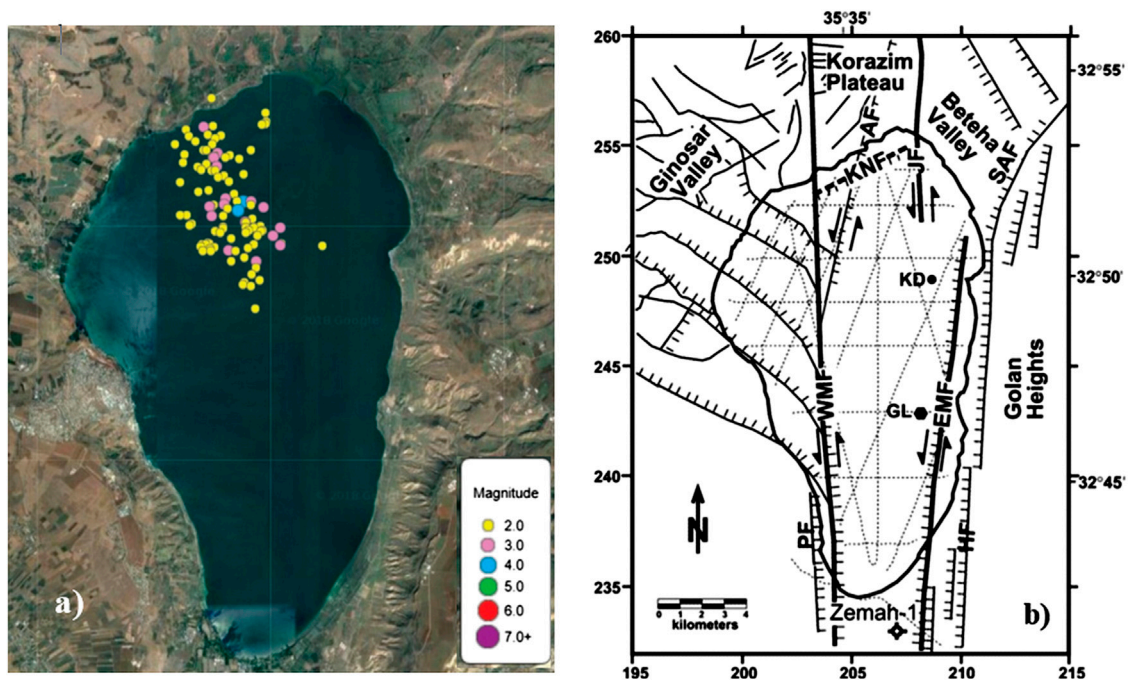


FIGURE 13 | (A) Accumulation of 103 earthquakes in the Dead Sea seismogenic active faults at the bottom of Lake Kinneret, which were recorded during the 2018 summer between 4 July and 18 August. **(B)** The tectonic map showing the internal structure of the lake (Hurwitz et al., 2002). EMF and WMF are the eastern and western marginal faults, KNF is the Kfar Nahum fault, and JF and AF are the Jordan and Almagor faults.

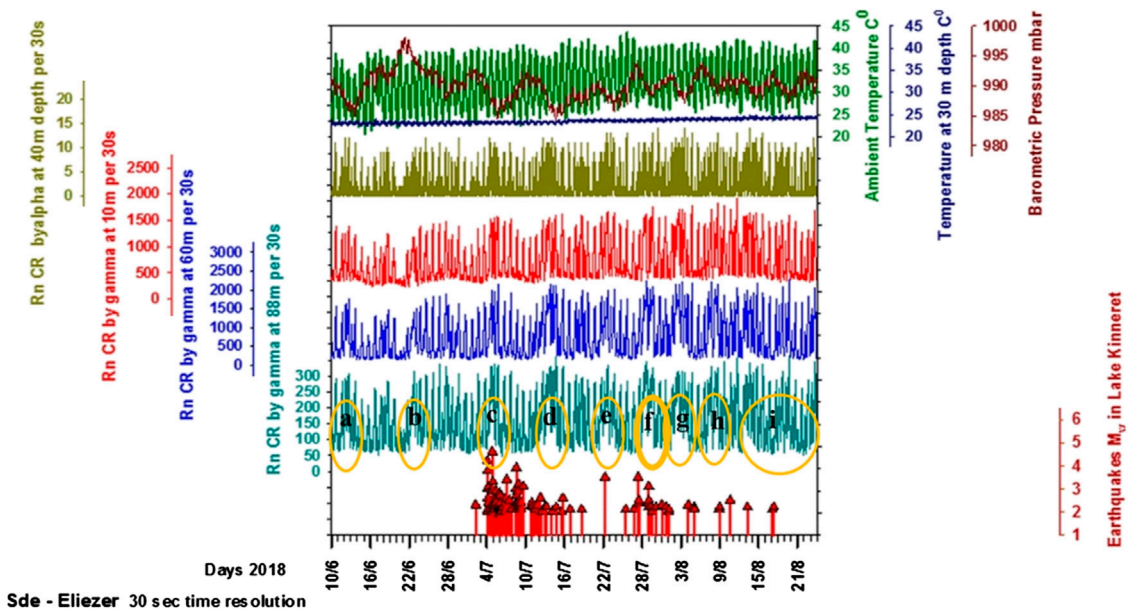


FIGURE 14 | Time series interval of 75 consecutive days at the Sde-Eliezer site. The Sde-Eliezer site is located about 35 km north of Lake Kinneret that was under weak seismic activity during July and August 2018. The **non-periodic, broader than 20 h signals**, on 12 (a) and 22 (b) June, 4 (c), 13 (d), 22 (e), and 28 & 29 (f) July, and 2 (g), 7 & 8 (h), and 12&13 (i) August, may reveal the pre-seismic progression of several weak geodynamic events in depth (details in Figures 24, and 25). In this figure, 0.1 counts per 30 s of the gamma sensors at 10, 60 and 88 m, are equivalent to concentration of 1 Bq/m³ within the surrounding country rock, and 0.0015 counts per 30 s of the alpha particle detector is equivalent also to 1 Bq/m³.

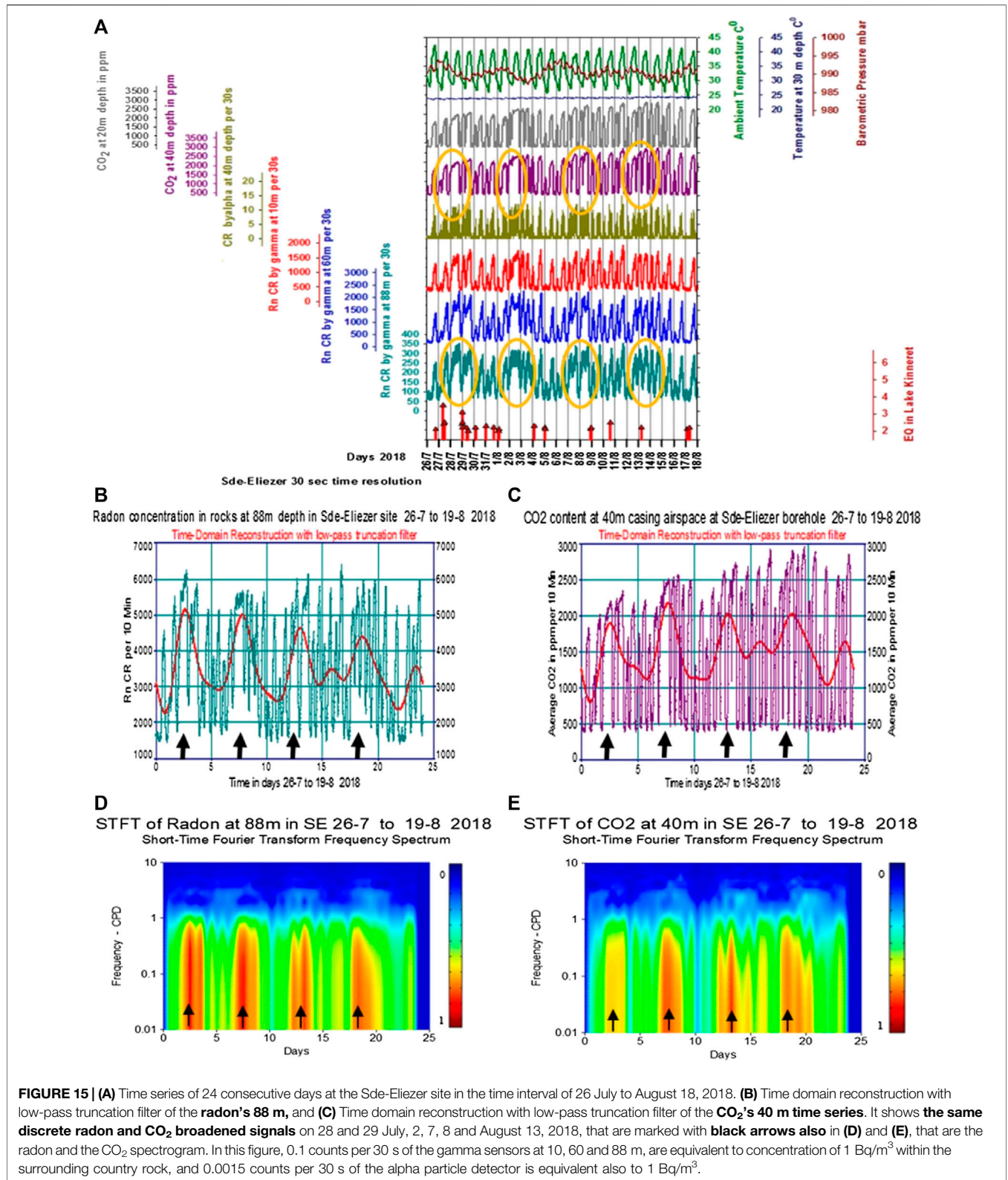


FIGURE 15 | (A) Time series of 24 consecutive days at the Sde-Eliezer site in the time interval of 26 July to August 18, 2018. **(B)** Time domain reconstruction with low-pass truncation filter of the radon's 88 m, and **(C)** Time domain reconstruction with low-pass truncation filter of the CO₂'s 40 m time series. It shows **the same discrete radon and CO₂ broadened signals** on 28 and 29 July, 2, 7, 8 and August 13, 2018, that are marked with **black arrows** also in **(D)** and **(E)**, that are the radon and the CO₂ spectrogram. In this figure, 0.1 counts per 30 s of the gamma sensors at 10, 60 and 88 m, are equivalent to concentration of 1 Bq/m³ within the surrounding country rock, and 0.0015 counts per 30 s of the alpha particle detector is equivalent also to 1 Bq/m³.

- **Case a:** happened on June 2015 and it was described in the previous “Phase IV: Impact of Atmospheric Aspects on Radon Transportation Within Porous Media” section and display in **Figures 12A,B**.
- **Case b:** happened on May 16, 2016, a radon anomalous signal preceding by 14 h the Nuweiba, $M = 5.1$ earthquake as displays in **Figures 12C,D**.
- **case c:** happened on 17 and July 23, 2016, two broadened anomalous radon signals appeared 7 and 2 days before the Palmyra Syria $M 4.5$ earthquake on 25 July 01:30 AM, as displays in **Figures 12E,F**.

Utilizing an existing algorithm that work in the frequency domain for low-pass truncation, frequency components above a chosen ideal cutoff frequency can be removed from the original radon time series, leaving the frequencies below it unaltered as well as any non-periodic discrete events. Choosing a frequency cutoff less the diurnal one (1 cycle per day) excludes all the unwanted diurnal, semidiurnal, and higher periodical signals (maybe harmonics) that are induced by the atmospheric parameters (e.g., **Figures 12G,H**).

The Second Period From May 2017 to End of 2018—Radon and CO₂ in Depth

Overview

In the middle of 2017, the setup at the Sde-Eliezer site was expanded to study the impact of atmospheric variables, (ambient pressure and temperature) on air flow within the deep dry borehole at the site—110 m deep and 1 m wide (Levintal et al., 2018). Temperature, relative humidity, CO₂ (at 5, 20, 40, and 70 m), and radon detectors (measured by gamma detectors at 10, 60, and 88 m and by alpha at 40 m) were placed along the cased boreholes (**Figures 8B** and **10A**) and barometric pressure probe was installed at the surface. Since then to present, all borehole data has been logged at a high 30 s temporal resolution.

Beyond that initially anticipated, the results show that CO₂ in the open borehole air space, as measured by four CO₂ detectors at different depths, follows the radon (measured by alpha detector at 40 m) as well as the radon temporal variations at the surrounding bedrocks (measured by gamma detectors at 10, 60, and 88 m), and both are driven by the climatic parameters as analyzed for the radon in our previous sections. Therefore, the CO₂ reveals the same daily and semi daily temperature and pressure periodicities in the frequency time domain (Zafir et al., 2019). Improving the sampling rate by 30 times (from 15 min to high 30 s resolution) and implementing four CO₂ detectors at different depths enabled measuring the CO₂ velocity in the Sde-Eliezer borehole under the influence of barometric pressure that seems to be more effective than temperature within the air space inside the open well (see “Phase VI: CO₂ and Rn-222 Emissions From an Abandoned Water Well Under the Influence of Climatic Pressure and Temperature” section).

Radon, CO₂, and Pre-Seismic Processes—The 2018 Lake Kinneret Scenario

In order to understand whether there is a link between earthquakes in the DSFZ and the gas signal measurements at

the depth in the abandoned well, located within the northern part of the fault belonging to the DSFZ (WMF in **Figure 13**), we have chosen to focus on the emergence of 103 seismic events in Lake Kinneret (Sea of Galilee) that occurred in the summer of 2018.

The temporal variations of the radon measurements at Sde-Eliezer site (located on the WMF about 35 km north of Lake Kinneret) and the rest of the environmental parameters, acquired simultaneously with all the earthquakes that occurred in the Lake Kinneret, are presented in **Figure 14**.

Despite the situation that the number of tremors were over 100, only two of them had magnitude of $M = 4.2$ and $M = 4.5$, and all the rest had lower magnitude between $M = 2$ and $M = 4$. Therefore, there was no early expectation that tectonic activity in the subsurface would be followed by a pre-seismic radon anomalous signals, as occurred before (The Recovery of a Pre-seismic Radon Anomalous Signal Apparently Associated With a Regional Geodynamic Process section). Nonetheless, about nine non-periodic radon signals, broader than 20 h each, have been exposed during 75 consecutive day from 10 June to 20 August (**Figure 14**).

The encircled segments designated as **a, b, c, d, e, f, g, h, i** in **Figure 14**, occurred within the time series in which the signals of radon are exceeding the daily and semi daily periodic effect of atmospheric temperature and pressure as analyzed by the FFT time domain reconstruction with low-pass truncation filter and short time Fourier transform (STFT) methods (for example see **Figure 15**). The results of the FFT filtering and the time domain reconstruction of the time section between 10 June and 12 July pinpointed the two anomalous peaks (**a**) and (**b**) in **Figure 14**, which started before the first rupture. It shows that two radon, clear, discreet, non-periodic and broadened with time duration that exceeds 20 h, on 12 and 22 June, preceding by 24 and 12 days the more powerful tremors of July 4, 2018, with magnitude $M = 4.5$.

A selected example in **Figure 15**, shows the analysis of the signals of radon and CO₂ during 24 consecutive days at the Sde-Eliezer site, from 26 July to August 18, 2018 including (**f**), (**g**), (**h**) and (**i**). The tremors in this time interval, fall below the magnitude of $M = 4$, and the relations between them and the gases temporal variations become non-diagnostic. There is a mixture of earthquakes on one hand and radon and CO₂ broadening signals, on the other. The broadened signals could probably be related to geodynamic activity as we have shown in the cases of earthquakes with magnitude above 4.5 (**Figures 12A–F**) but it is not possible to associated them to a specific event.

At least, based on our previous investigation on “Response of radon in a seismic calibration explosion” (“Overview” section), we suggest that there will be no an apparent response in the concentration of radon below the surface as a direct effect of short-time transient excess pressure produced by any one of the swarm’s earthquake, including the highest one of $M = 4.5$ on 4 July (**Figure 14**). It is also possible to assume that the phenomenon of dilation in the time of the CO₂ signals that occurs simultaneously with the extension of the radon signals (**Figure 15**), and of course independent with it, is genuine.

In general, any geodynamic process that causes stress or strain release affects subsurface fluids, irrespectively if the process will finally produce an earthquake or not.

SUMMARY AND CONCLUSIONS

In situ Monitoring of Subsurface Radon—Experimental Point of View

The long-term geophysical investigation of radon in shallow and deep boreholes, based on passive measuring systems (no pumping and gas circulation that disturb the local environmental equilibrium) was able to detect radon temporal changes, with very high sensitivity and high time resolution. It enabled the researchers to eliminate climatic-induced periodic contributions from the radon time series, and thus extract the part of the signals that could be correlated with regional geodynamic processes. The various monitoring systems that were found to be suitable for use in a passive way included various types of gamma and alpha detectors.

The basic principle to choose the gamma detection by SCA technique for total counting of RDPs' (radon decay products) gamma rays, is the assumption that radon is the only radioactive element that can vary in terms of its amount in the porous media under the impact of upper climatic or deeper geodynamic activities. These fluctuations are measurable as an additional increment to the measured gamma radiation from natural elements as uranium, thorium and potassium that form a constant background in time. This background also includes the contributions of all the RDPs atoms that remain confined inside the solid material and are not emanated to the porous media neither free to move under the influence of various driving forces.

Therefore, the variable contribution in the measurement of radon by the gamma detector does not actually exceed 10–25% of the total radiation that is measured. Thus, the first test for a system's performance is its capability to recover the daily changes in the temporal radon transport variation within a soil media, while the detector is lowered into ground depth of at least 2–5 m in an open area. It also needs to take into consideration that too lower radon contents do not allow to measure significant temporal variations in the concentration of radon, under the daily periodic behavior. Experimentally, it should be higher than 1 kBq/m³, few times above 200 Bq/m³, the average outdoor radon levels.

BGO and NaI gamma detectors were selected after being ascertained that they have high sensitivity, stability and suitability for use in a 2-inch diameter drilling holes to a depth of several dozen meters. We have also re-defined the energy range the SCA of the gamma detectors to count gamma rays between 475 and 3,000 keV, cancelling the measurement of gamma radiation in the field of the Compton scattering, between 50 and 450 keV, enabling to improve the ratio of signal to noise by 70% in comparison to the common detection systems (Figure 1A).

The main result was that gamma detectors have a higher sensitivity between 2 and 4 times in relation to the alpha detector, which enables them reveal to detect low sub-diurnal fluctuations. The construction of hermetic and water-protected housing enables the use of these radon gamma radiation detectors in a variety of environments such as soil, country rock, ground and seawater, and any subterranean spaces including drillings.

Discrimination Between the Influence of Climatic Temperature and Pressure on Radon Flow in Geological Media

Combined long-term radon measurement by gamma and alpha methods within deep abandoned boreholes empowered the capability to distinguish between radon anomalous signals at depth induced by temperature and barometric pressure. The main evidences of our research are:

1) The radon present in country rock formations that is measured by gamma radiation detectors is propelled by the surface temperature gradient to at least a proven depth of 100 m. The radon reveals a daily periodicity similar to the one per day cycle of the surface temperature. The gamma detector at each level, presents very sharp, clear and accurate peaks as a result of a high counting rate and low error, with a specific time lag between each other. It was found that the time lag depends on the downward radon velocity within the bedrock type.

The list of results that includes measurement from different monitoring sites is as follows:

- At Sde Eliezer site, Israel, a time lag of 2 h was measured between 10 and 60 m depth, implying a downward radon velocity of 25 m per h (Zafir et al., 2016).
- At Nachal Mor site, Israel, a time lag of 2 h was measured between 10 and 40 m depth implying a downward radon velocity of 15 m per h (Zafir et al., 2019).
- At Amram tunnel site, Israel, a time lag of 10 h was measured, between 0 and 100 m depth implying a downward radon velocity of 10 m per h (Zafir et al., 2013).
- At Bentonite mine, in Makhtesh Ramon, Israel, a time lag of 5 h was measured between 0 and 40 m depth, implying a downward radon velocity of 8 m per h (Zafir and Malik, 2010).
- At Ghuttu site in Garhwal Himalaya, India, a time lag of 3 h was measured between 0 and 10 m depth, implying a downward radon velocity of 3.3 m per h (Choubey et al., 2011).

In general, from a geophysical point of view, there was no need to find any other gases that would bear radon up or down (e.g. Etiope and Martinelli, 2002; Neri et al., 2016). Once the Sun surface heating provides energy to the radon atoms their ballistic moment (mv) downward is at least 4 times larger than any other natural gas atoms. The same process can lead to the emergence of radon and other gases, close to the surface, under the effects of underground heating associated with volcanic events.

2) The radon concentration within any open underground space, such as an abandoned drilling, as measured by a detector of its alpha particles, is controlled by the negative barometric pressure gradient (in anti-correlation).

3) Most of the radon daily signals that are recognized as induced by climatic parameters, appear once or twice a day at specific times: early morning and afternoon (e.g., 4–6 AM and 5–7 PM, in 60 m depth at Sde-Eliezer site, Figure 9C).

4) The amplitudes of the radon periodical signals are controlled by the intensity of the climatic driving force, in

linear dependency with the pressure gradient according to the existing physical model, and with largest non-linear variations induced by the ambient temperature gradient, that according to the ratio between the radon level in winter to summer varies by a factor of 3–10 while the temperature varies within 10% span (28 change vs. 285 K).

These phenomenological indications cause difficulties in accepting the results of any statistical analysis that is based on daily, multi-day, seasonal and multi-year averages calculations, of the radon gas levels in any media. Since the half-life of radon is short and constant (3.8 days), and naturally it always tends to be in secular equilibrium, only external driving forces will cause the radon to move within the geological media. Hence, such calculations actually reveal and reflect the temporal variations of the external climatic parameters, the ambient temperature and pressure, which undulate a combined change of the amplitude of the radon signal during daily scale, multi-day variation and significant changes between seasons too. This assumption is undoubtedly correct when the radon gas detector is installed at a shallow depth of a few dozen centimeters.

In addition to the difference in the intensity of the radon signals between the summer and winter, it is also possible to discern in all the above works, the multi day heat waves, mainly in the spring and summer, that are simultaneously producing waves of radon that are prolonging within the same time (e.g., **Figures 6A,B**). Over these heat waves there are exposed signals in a daily cycle with a peak that follows the maximum of the daily temperature, with a delay in time depending on the depth of the detector. The same phenomena can be observed with barometric pressure waves lasting few days that also affect the continuous level of the radon under the surface in addition to the semidaily and diurnal signals (**Figure 7B**). It is important to emphasize that the two phenomena with daily and multi-day variations, are not always dependent on each other, as for example, the semi-daily cycle that exists only in the periodicity of barometric pressure, prompted by an atmospheric tide (Zafir et al., 2013).

Therefore, it is impossible to separate the influence of the climatic driving force by additive arithmetic operations. For example, the subtraction of the moving average of 7 days from the daily average as part of the statistical manipulation to calculate anomalies higher than twice the standard deviation is uncertain and problematic (e.g., Ghosh et al., 2009; Cannelli et al., 2016; Singh et al., 2017; Barkat et al., 2018; Alam et al., 2020). Even the attempt to adapt regression equations to radon time series utilizing every environmental variable and generating a best linear regression model to correlate between radon variations and meteorological parameters, does not enable to resolve and defined the subsurface contribution to the anomalous radon temporal variation (Neri et al., 2016).

5) There can be a number of ways for analyzing, identifying the nature of the anomalies in the measured time series, dismount to various components, and isolating the parameters operating as driving forces for the radon movements beneath the surface. The **convolution** is a mathematical procedure of combining different signals to form an another signal, or isolate components and detect signals with filtering and reconstruction techniques. It is the single and most important technique in Digital Signal Processing (e.g., Smith, 2002).

Although, there is no yet explicit mathematical expression for the thermal gradient rule in the radon transportation process, to be insert within the convolution integral, one can use the Fourier analysis to convert signals from their original time domain to a presentation in the frequency domain and vice versa.

We apply the Fourier domain filtering and component isolation procedure (by AutoSignal™ of Systat Software Inc.). Utilization of an existing algorithm that work in the frequency domain for low-pass truncation of frequency components above a chosen ideal cutoff frequency, enabled to remove them from the original radon time series, leaving the frequencies below it unaltered as well as any non-periodic discrete events. Choosing a frequency cutoff less the diurnal (one cycle per day), excludes all the unwanted diurnal, semidiurnal, and higher periodical signals (maybe harmonics) that are induced by the atmospheric parameters and proved that indeed we measured radon anomaly that its emergence lasts for more than 20 h and that these non-cyclical signals may precede by several hours or more a forthcoming seismic events even if they are weak.

It is important to note that according to our ongoing experience, the broad signals associated with tectonic activity almost cannot be revealed even by the measurements of radon temporal variation at 10 m depth. It was easy to observe within the long-time series acquired during the last 4 years, that the entire radon measured signals at the shallow depth of 10 m, used as reference for the deep data acquisition, are mostly radon periodical signals produced under the direct effect of the climatic driving forces on the ground surface.

As long as investigations continue to rely on detectors installed at a depth that does not exceed 10 m, the likelihood of discovering non-cyclical signals associated with tectonic activity in depth remains slim.

Currently, it is clear that there are gaps in our knowledge, including depths, time scale, range and magnitude of the energy release by pre-seismic geophysical processes and the relationship between radon temporal behavior and these various tectonic processes. Moreover, it seems that there is no proof for the assumption that the radon signal induced by seismo-tectonic processes has to appear with an intensity higher than the climatic-induced periodic signal, except in the case of a high-magnitude earthquake and a measuring system that is located near the event, such as occurred in Kobe, Japan (M = 7.2 at 30 km distance, Igarashi et al., 1995).

Radon, CO₂ and Other Natural Gas in Depth as a Proxy for Investigating Tectonic Pre-seismic Activity

As observed in the Sde Eliezer results, radon signals that are induced by the ambient temperature and pressure have diurnal and semidiurnal periodicity and amplitudes which are variable and not uniform. In general, they preserve the multiday profiles of the atmospheric temperature and barometric pressure as well. Monitoring radon at a depth of several dozen meters, substantially attenuates the climatic contribution and increases the possibility of resolving from the radon temporal spectrum the

preseismic radon signals that are not periodic and are independent from the atmospheric driving forces.

In parallel it was observed that CO₂, within the internal airspace of the borehole at Sde Eliezer, within various depth (5, 20, 40, and 70 m) follows the radon (measured by alpha detector at 40 m) as well as the radon temporal variations at the surrounding bedrock (measured by gamma detectors at 10, 60, and 88 m), and both are driven by the climatic parameters as analyzed for radon (e.g., **Figure 15**). Thus, CO₂ reveals the same daily and semi daily temperature and pressure periodicities in the frequency time domain and clearly responds, simultaneously with radon, to the apparently tectonic pre-seismic driving force, with the same rise, fall, and broadening times.

Improving the sampling rate by 30 times (from 15 min to high 30 s resolution) and implementing four CO₂ detectors at different depths enabled measuring the CO₂ velocity in the Sde-Eliezer borehole under the influence of barometric pressure that seems to be more effective than temperature within the air space inside the open well (Levintal et al., 2020).

Similar to radon, the high CO₂ concentration above the atmospheric content (about 400 ppm) and up to 2,800 ppm at Sde-Eliezer site, entered the sealed borehole's iron casing through the perforated lower sections below 80 m, and then degassing into the sealed casing from the water table. The source of the high CO₂ content could be the microbial activity within the vadose zone, or the presence of an organic substance (peat/lignite) trapped in the Hula Valley's bedrock. Hence, it is reasonable to assume the same thermodynamic mechanism supplies CO₂ as well as radon to the groundwater.

The above conclusion means that the two gases, radon and CO₂ are driven down within the geological media by the combined temperature ΔT and pressure ΔP gradients. Therefore, they reveal the same daily and semi-daily periodicity (**Figure 15**).

Now, it is expected that recovering of non-periodic broadening of radon and CO₂ signals, enables eliminating the climatic-induced periodic contributions and extract the residual portion of the radon and CO₂ signals related to the regional tectonic pre-seismic processes, and could be used as earthquake precursors before the main rupture occurs. It is not essential that each one of these geodynamic processes will end as an earthquake.

In order to use the CO₂ temporal variations as a proxy for pre-seismic activity its concentration within the geological media, should be at least twice as high as the atmospheric contents of about 400 ppm. Otherwise, any change will only be a fluctuation of the atmospheric concentration by few tens of ppm under the influence of the barometric pressure, as measured at Nachal Mor site (Zafir et al., 2019) or even reaching lower levels as 200 ppm in isolated tunnels as in Amram site (Zafir et al., 2013). The results at Nachal Mor for example, prove that there are no organic materials in rocks and soil around the Dead Sea and they are not the source of radon there either (Kronfeld et al., 1991).

Another important result that emerged is our deep gas monitoring technology. The technology may become a useful tool for the investigation of seismic precursors since similarly to

radon and CO₂, the existence of any natural gas such as nitrogen, oxygen, methane, hydrogen sulfide, carbon monoxide and helium within deep subsurface media can serve as a proxy for pre-seismic precursory phenomena.

In general, any geodynamic process that causes stress or strain release affects subsurface fluids, irrespectively if the process will finally produce an earthquake or not.

DATA AVAILABILITY STATEMENT

The raw data supporting the conclusions of this article will be made available by the authors, without undue reservation.

AUTHOR CONTRIBUTIONS

H.Z. Conceptualization, Methodology, Fieldwork, Writing – original draft, Data Analysis, and Presentation. S.B. Conceptualization, Methodology, Writing, Review & editing, and Data analysis. E.L. Conceptualization, Methodology, Fieldwork, Formal analysis. N.W. Supervision, Conceptualization, Methodology, and Review. Y.H. Conceptualization, Methodology, Seismology and Data analysis. Z.Z. Conceptualization, Methodology, Data analysis and Methods, and Review.

ACKNOWLEDGMENTS

The authors would like to thank Dr Heiko Woith and Dr Vivek Walia for the very careful, constructive and throughout review and for the significantly improving the clarity and the quality of this paper. The authors would like to gratefully thank and honor Mr. Haim Hemo who worked for many years at the Geological Survey of Israel (GSI) and passed away in October 2018. He was a tireless worker and a supporting pillar in all of the field work since 2012. The authors acknowledge and honor Dr Gideon Steinitz who also passed away in July 2017 for the cooperation offered to the team, allowing to perform the research, from 2007 to 2012, within the partially supporting funds the Ministry of Energy of Israel (grants 25-017-13, 27-17-058, 28-17-011, 29-17-004), and for constructive and valuable joint discussions on radon as natural tracer in general, and for cooperating with the publication of the two manuscripts in 2009 and 2011, in particular. Mr. Uri Malik from GSI and Mr. Raz Amir from Ben-Gurion University of the Negev assisted in the data collection and the field work. Many thanks to Dr Yossi Guttman from Mekorot Israel National Water Co., Tel-Aviv, Israel, for the permission to install the research system in the abandoned water well at Sde-Eliezer site in The Hula Valley. The data used in this study were acquired also in the framework of activity supported by the Ministry of Energy, Israel (grant 216-17-010, and 11-17-2012).

REFERENCES

- Aharonov, E., and Scholz, C. H. (2018). A physics-based rock friction constitutive law: steady state friction. *J. Geophys. Res. Solid Earth*. 123, 1591–1614. doi:10.1002/2016jb013829
- Akerblom, G., Andersson, P., and Clevenstjöm, B. (1984). Soil gas radon—a source for indoor radon daughters. *Radiat. Protect. Dosim.* 7, 49–54. doi:10.1093/oxfordjournals.rpd.a082961
- Alam, A., Wang, N., Zhao, G., and Barkat, A. (2020). Implication of radon monitoring for earthquake surveillance using statistical techniques: a case study of Wenchuan earthquake. *Geofluids* 2020, 14. doi:10.1155/2020/2429165
- Al-Zoubi, A. S., Abu-Hamattah, Z. S. H., and Abdealkader, A. (2006). The seismic hazard assessment of the Dead Sea rift, Jordan. *J. Afr. Earth Sci.* 45, 489–501. doi:10.1016/j.jafrearsci.2006.04.007
- Atkins, M. L., Santos, I. R., Perkins, A., and Maher, D. T. (2016). Dissolved radon and uranium in groundwater in a potential coal seam gas development region (Richmond River Catchment, Australia). *J. Environ. Radioact.* 154, 83–92. doi:10.1016/j.jenvrad.2016.01.014
- Barberio, M., Gori, F., Barbieri, M., Billi, A., Devoti, R., Doglioni, C., et al. (2018). Diurnal and semidiurnal cyclicity of radon (222Rn) in groundwater, giardino spring, central apennines, Italy. *Water* 10, 1276. doi:10.3390/w10091276
- Barbosa, S. M., Zafir, H., Malik, U., and Piatibratova, O. (2010). Multiyear to daily radon variability from continuous monitoring at the Amram tunnel, southern Israel. *Geophys. J. Int.* 182 (2), 829–842. doi:10.1111/j.1365-246x.2010.04660.x
- Barkat, A., Ali, A., Hayat, U., Crowley, Q. G., Rehman, K., Siddique, N., et al. (2018). Time series analysis of soil radon in Northern Pakistan: implications for earthquake forecasting. *Appl. Geochem.* 97, 197–208. doi:10.1016/j.apgeochem.2018.08.016
- Cannelli, V., Piersanti, A., Galli, G., and Melini, D. (2018). Italian radon monitoring network (IRON): a permanent network for near real-time monitoring of soil radon emission in Italy. *Ann. Geophys.* 61 (4), 444. doi:10.4401/ag-7604
- Cannelli, V., Piersanti, A., Spagnuolo, E., and Galli, G. (2016). Preliminary analysis of radon time series before the M=6 Amatrice earthquake: possible implications for fluid migration. *Ann. Geophys.* 59, 1–7. doi:10.4401/ag-7166
- Choubey, V. M., Arora, B. R., Barbosa, S. M., Kumar, N., and Kamra, L. (2011). Seasonal and daily variation of radon at 10m depth in borehole, Garhwal Lesser Himalaya, India. *Appl. Radiat. Isot.* 69 (7), 1070–1078. doi:10.1016/j.apradiso.2011.03.027
- Cicerone, R. D., Ebel, J. E., and Britton, J. (2009). A systematic compilation of earthquake precursors. *Tectonophysics* 476, 371–396. doi:10.1016/j.tecto.2009.06.008
- Cigna, A. (2005). Radon in caves. *Int. J. Speleol.* 34, 1. doi:10.5038/1827-806X.34.1.1
- Dai, A., and Wang, J. (1999). Diurnal and semidiurnal tides in global surface pressure fields. *J. Atmos. Sci.* 56, 3874–3891. doi:10.1175/1520-469(1999)056<3874:DASTIG>2.0.CO;2. doi:10.1175/1520-0469(1999)056<3874:dastig>2.0.co;2
- Eff-Darwich, A., Martín-Luis, C., Quesada, M., de la Nuez, J., and Coello, J. (2002). Variations on the concentration of 222Rn in the subsurface of the volcanic island of Tenerife, Canary Islands. *Geophys. Res. Lett.* 29 (22), 26. doi:10.1029/2002GL015387
- Etiopie, G., and Martinelli, G. (2002). Migration of carrier and trace gases in the geosphere: an overview. *Phys. Earth Planet. Inter.* 129, 185–204. doi:10.1016/S0031-9201(01)00292-8
- Falsaperla, S., Neri, M., Di Grazia, G., Langer, H., and Spampinato, S. (2017). What happens to in-soil Radon activity during a long-lasting eruption? Insights from Etna by multidisciplinary data analysis. *G-cubed* 18, 2162. doi:10.1002/2017GC006825
- Fleischer, R. L. (1981). Dislocation model for radon response to distant earthquakes. *Geophys. Res. Lett.* 8 (5), 477–480. doi:10.1029/GL008i005p00477
- Fleischer, R. L., Turner, R. G., and George, A. C. (1984). Passive measurement of working levels and effective diffusion constants of radon daughters by the nuclear track technique. *Health Phys.* 47 (1), 9–19. doi:10.1097/00004032-198407000-00001
- Fu, C.-C., Walia, V., Yang, T. F., Lee, L.-C., Liu, T.-K., Chen, C.-H., et al. (2017). Preseismic anomalies in soil-gas radon associated with 2016 M 6.6 Meinong earthquake, Southern Taiwan. *Terr. Atmos. Ocean Sci.* 28, 787–798. doi:10.3319/TAO.2017.03.22.01
- Fujiyoshi, R., Sakamoto, K., Imanishi, T., Sumiyoshi, T., Sawamura, S., Vaupotic, J., et al. (2006). Meteorological parameters contributing to variability in 222Rn activity concentrations in soil gas at a site in Sapporo, Japan. *Sci. Total Environ.* 370, 224–234. doi:10.1016/j.scitotenv.2006.07.007
- George, A. C. (1984). Passive, integrated measurement of indoor radon using activated carbon. *Health Phys.* 46 (4), 867–872. doi:10.1097/00004032-198404000-00012
- George, A. C. (1990). An overview of instrumentation for measuring environmental radon and radon progeny. *IEEE Trans. Nucl. Sci.* 37, 892–901. doi:10.1109/23.106733
- Ghosh, D., Deb, A., and Sengupta, R. (2009). Anomalous radon emission as precursor of earthquake. *J. Appl. Geophys.* 69, 67–81. doi:10.1016/j.jappgeo.2009.06.001
- Gitterman, Y., Hofstetter, A., and Pinsky, V. (2005). (GII) Report No. 554/163/05. Beit-alfa calibration experiment. Geophysical Institute of Israel.
- Groves-Kirkby, C. J., Denman, A. R., Crockett, R. G. M., and Phillips, P. S. (2004). "Periodicity in domestic radon time series—evidence for earth tides," in 11th International congress of the international radiation protection association (IRPA11-6a27), Madrid, Spain, May 23–28, 2004.
- Hakl, J., Csige, I., Hunyadi, I., Várhegyi, A., and Géczy, G. (1996). Radon transport in fractured porous media - experimental study in caves. *Environ. Int.* 22 (1), 433–437. doi:10.1016/S0160-4120(96)00143-2
- Hassan, N. M., Hosoda, M., Ishikawa, T., Sorimachi, A., Sahoo, S. K., Tokonami, S., et al. (2009). Radon migration process and its influence factors; review. *Jpn. J. Health Phys.* 44 (2), 218–231. doi:10.5453/jhps.44.218
- Hurwitz, S., Garfunkel, Z., Ben-Gai, Y., Reznikov, M., Rotstein, Y., and Gvirtzman, H. (2002). The tectonic framework of a complex pull-apart basin: seismic reflection observations in the Sea of Galilee, Dead Sea transform. *Tectonophysics* 359, 289–306. doi:10.1016/S0040-1951(02)00516-4
- Ichitsubo, H., and Yamada, Y. (2004). Effect of a grounded object on radon measurement using AlphaGUARD. *Health Phys.* 87 (1), 79–81. doi:10.1097/00004032-200407000-00010
- Igarashi, G., Saeki, S., Takahata, N., Sumikawa, K., Tasaka, S., Sasaki, Y., et al. (1995). Ground-water radon anomaly before the Kobe earthquake in Japan. *Science* 269, 60–61. doi:10.1126/science.269.5220.60
- Ivanovich, M., and Harmon, R. S. (Editors) (1982). *Uranium-series disequilibrium: applications to environmental problems*. Oxford, UK: Oxford Science Publications, 1–32.
- Jönsson, G. (1997). The nuclear track detector—a tool in radon measurements. *Radiat. Meas.* 28 (6), 695–698. doi:10.1016/S1350-4487(97)00166-2
- King, C.-Y. (1986). Gas geochemistry applied to earthquake prediction: an overview. *J. Geophys. Res.* 91, 12269–12281. doi:10.1029/jb091ib12p12269
- Knoll, G. F. (2000). *Radiation detection and measurement*. Hoboken, NJ, USA, John Wiley & Sons.
- Koch, U., and Heinicke, J. (1996). Radon behavior in mineral spring water of bad brambach (vogtland, Germany) in the temporal vicinity of the 1992 Roermond earthquake, the Netherlands. *Int. J. Rock Mech. Min. Sci. Geomech. Abstr.* 33, 5A. doi:10.1016/0148-9062(96)87376-1
- Kockum, S. W. (2002). *Digital signal processing: a practical guide for engineers and scientists*. Oxford, UK: Newnes Publ., ISBN 0-7506-7444-X.
- Kronfeld, J., Ilani, S., and Strull, A. (1991). Radium precipitation and extreme 238U-series disequilibrium along the Dead Sea coast, Israel. *Appl. Geochem.* 6, 355–361. doi:10.1016/0883-2927(91)90011-d
- Levintal, E., Dragila, M. I., Zafir, H., and Weisbrod, N. (2020). The role of atmospheric conditions in CO₂ and radon emissions from an abandoned water well. *Sci. Total Environ.* 722, 137857. doi:10.1016/j.scitotenv.2020.137857
- Levintal, E., Zafir, H., Dragila, M. I., and Weisbrod, N. (2018). The role of atmospheric conditions in driving air movement along a deep borehole using radon and CO₂ mutual relation. *Geophys. Res. Abstr.* 20, 6075.
- Lucas, H. F. (1957). Improved low-level alpha scintillation counting for radon. *Rev. Sci. Instrum.* 68, 680–683. doi:10.1148/68.2.258
- Martin-Luis, M. C., Steinitz, G., Soler, V., Quesada, M. L., and Casillas, R. (2015). 222Rn and CO₂ at las cañadas caldera (Tenerife, Canary islands). *Eur. Phys. J. Spec. Top.* 224 (4), 641–657. doi:10.1140/epjst/e2015-02397-7

- Mentes, G., and Eper-Pápai, I. (2015). Investigation of temperature and barometric pressure variation effects on radon concentration in the Sopronbánfalva Geodynamic Observatory, Hungary. *J. Environ. Radioact.* 149, 64–72. doi:10.1016/j.jenvrad.2015.07.015
- Mogro-Campero, A., and Fleischer, R. L. (1977). Subterrestrial fluid convection: a hypothesis for long distance migration of radon within the earth. *Earth Planet Sci. Lett.* 34, 321–325. doi:10.1016/0012-821X(77)90017-6.
- Monnin, M., Morin, J. P., and Seidel, J. L. (1993). A comprehensive approach of radon measurements for geophysical studies. *Nucl. Tracks Radiat. Meas.* 22(4), 403–411. doi:10.1016/0969-8078(93)90095-1
- Muga, J. (2017). Geochemical assessment for morendat East geothermal prospect, using radon and carbondioxide concentration from soil, Kenya. *J. Geol. Resour. Eng.* 1, 38–47. doi:10.17265/2328-2193/2017.01.004.
- Muramatsu, H., Tashiro, Y., Hasegawa, N., Misawa, C., and Minami, M. (2002). Seasonal variations of ²²²Rn concentrations in the air of a tunnel located in Nagano city. *J. Environ. Radioact.* 60, 263–274. doi:10.1016/s0265-931x(01)00085-6
- Neri, M., Ferrera, E., Giammanco, S., Currenti, G., Cirrincione, R., Patanè, G., et al. (2016). Soil radon measurements as a potential tracer of tectonic and volcanic activity. *Sci. Rep.* 6, 24581. doi:10.1038/srep24581
- Nield, D. A., and Bejan, A. (2006). *Convection in porous media*. New York: Springer. ISBN 978-1-4614-5541-7.
- Noguchi, M., and Wakita, H. (1977). A method for continuous measurement of radon in groundwater for earthquake prediction. *J. Geophys. Res.* 82, 1353–1357. doi:10.1029/jb082i008p01353
- Oh, Y., and Kim, G. (2015). A radon-thoron isotope pair as a reliable earthquake precursor. *Sci. Rep.* 5, 13084. doi:10.1038/srep13084.
- Percival, D. B. (2008). “Analysis of geophysical time series using discrete wavelet transforms: an overview,” in *Lecture notes in Earth Sciences*. Editors R. V. Donner and S. M. Barbosa (Berlin, Germany: Springer), 112, 61–79. ISBN 978-3-540-78937-6.
- Perrier, F., and Girault, F. (2013). Harmonic response of soil radon-222 flux and concentration induced by barometric oscillations. *Geophys. J. Int.* 195 (2), 945–971. doi:10.1093/gji/ggt280.
- Pinault, J. L., and Baubron, J. C. (1996). Signal processing of diurnal and semi-diurnal variations in Radon and atmospheric pressure, moisture, and soil temperature data: a new approach for radon concentration modeling. *J. Geophys. Res.* 101 (B2), 31573171. doi:10.1029/95jb03121
- Przylibski, T. A. (2001). Radon and its daughter products behavior in the air of an underground tourist route in the former arsenic and gold mine in zloty stok (Sudety Mountains, SW Poland). *J. Environ. Radioact.* 57 (1), 87–103. doi:10.1016/s0265-931x(01)00012-1
- Richon, P., Perrier, F., Sabroux, J.-C., Trique, M., Ferry, C., Voisin, V., et al. (2005). Spatial and time variations of radon-222 concentration in the atmosphere of a dead-end horizontal tunnel. *J. Environ. Radioact.* 78 (2), 179–198. doi:10.1016/j.jenvrad.2004.05.001
- Riggio, A., and Santulin, M. (2015). Earthquake forecasting: a review of radon as seismic precursor. *Boll. Geofis. Teorica.* 56 (2), 95–114. doi:10.4430/bgta0148
- Rogers, V. C., and Nielson, K. K. (1991). Multiphase radon generation and transport in porous materials. *Health Phys.* 60, 807–815. doi:10.1097/00004032-199106000-00006
- Sahu, P., Panigrahi, D. C., and Mishra, D. P. (2016). A comprehensive review on sources of radon and factors affecting radon concentration in underground uranium mines. *Environ. Earth Sci.* 75, 617. doi:10.1007/s12665-016-5433-8
- Schubert, M., and Schulz, H. (2002). Diurnal radon variations in the upper soil layers and at the soil-air interface related to meteorological parameters. *Health Phys.* 83 (1), 91–96. doi:10.1097/00004032-200207000-00010
- Siino, M., Scudero, S., Cannelli, V., Piersanti, A., and D’Alessandro, A. (2019). Multiple seasonality in soil radon time series. *Sci. Rep.* 9, 8610. doi:10.1038/s41598-019-44875-z
- Singh, S., Jaishi, H. P., Tiwari, R. P., and Tiwari, R. C. (2017). Time series analysis of soil radon data using multiple linear regression and artificial neural network in seismic precursory studies. *Pure Appl. Geophys.* 174, 2793–2802. doi:10.1007/s00024-017-1556-4
- Skeltan, A., Andrén, M., Kristmannsdóttir, H., Stockmann, G., Mörth, C.-M., Sveinbjörnsdóttir, Á., et al. (2014). Changes in groundwater chemistry before two consecutive earthquakes in Iceland. *Nat. Geosci.* 7, 752–756. doi:10.1038/ngeo2250
- Steinitz, G., Begin, Z. e. B., and Gazit-Yaari, N. (2003). Statistically significant relation between radon flux and weak earthquakes in the Dead Sea rift valley. *Geol.* 31, 505–508. doi:10.1130/0091-7613(2003)031<0505:ssrbf>2.0.co;2
- Steinitz, G., and Piatibratova, O. (2009). Radon signals in the gavnunim intrusion, Makhtesh Ramon, Israel. *Geophys. J. Int.* 180 651665. doi:10.1111/j.1365-246X.2009.04450.x.
- Steinitz, G., Piatibratova, O., and Barbosa, S. M. (2007). Radon daily signals in the elat granite, southern Arava, Israel. *J. Geophys. Res.* 112, B10211. doi:10.1029/2006JB004817.
- Steinitz, G., Vulkan, U., Lang, B., Gilat, A., and Zafir, H. (1992). Radon emanation along border faults of the rift in the Dead Sea area. *Isr. J. Earth Sci.* 41, 9–20.
- Torres-González, P., Moure-García, D., Luengo-Oroz, N., Villasante-Marcos, V., Soler, V., Iribarren, I. E., et al. (2019). Spatial and temporal analysis of temperature and gaseous emission inside a gallery in an active volcanic island (tenerife, canary islands). *Pure Appl. Geophys.* 176, 3467. doi:10.1007/s00024-019-02174-8
- Trique, M., Richon, P., Perrier, F., Avouac, J. P., and Sabroux, J. C. (1999). Radon emanation and electric potential variations associated with transient deformation near reservoir lakes. *Nature* 399, 137–141. doi:10.1038/20161
- Van der Spoel, W. H. (1998). Radon transport in sand: a laboratory study. PhD thesis. Eindhoven (The Netherlands): Technical University Eindhoven.
- Van der Spoel, W. H., Van der Graaf, E. R., and de Meijer, R. J. (1998). Combined diffusive and advective transport of radon in a homogeneous column of dry sand. *Health Phys.* 74, 48–63. doi:10.1097/00004032-199801000-00006
- Vaupotič, J., Riggio, A., Santulin, M., Zmazek, B., and Kobal, I. (2010). Radon anomaly in soil gas at Cazzaso, NE Italy, as a precursor of an ML = 5.1 earthquake. *Nukleonika* 55 (4), 507–511.
- Vulkan, U., Lang, B., and Steinitz, G. (1995). Electronic monitoring of radon in soil and water at the Northwestern Dead Sea area, first results. *Isr. Geol. Surv. Rep. GSI/45/95*, and SNRC Rep. ZD/179/95.
- Vulkan, U., Steinitz, G., Strull, A., and Zafir, H. (1992). Long-distance (+100 m) transport of radon in syenitic rocks at Makhtesh Ramon, Israel. *J. Nucl. Geophys.* 6 (2), 261–271. ISSN 0886-0130.
- Walia, V., Virk, H. S., Yang, T. F., Mahajan, S., Walia, M., and Bajwa, B. S. (2005). Earthquake prediction studies using radon as a precursor in N-W himalayas, India: a case study. *Terr. Atmos. Ocean Sci.* 16 (4), 775–804. doi:10.3319/tao.2005.16.4.775(gig)
- Wang, C.-Y., and Manga, M. (2010). Hydrologic responses to earthquakes and a general metric. *Geofluids* 10, 206–216. doi:10.1111/j.1468-8123.2009.00270.x
- Weinberger, R., Gross, M. R., and Sneh, A. (2009). Evolving deformation along a transform plate boundary: example from the Dead Sea Fault in northern Israel. *Tectonics* 28 (5), 1–19. doi:10.1029/2008tc002316
- Wertheim, D., Gillmore, G., Brown, L., and Petford, N., (2010). A new method of imaging particle tracks in solid state nuclear track detectors. *J. Microsc.* 237, 1–6. doi:10.1111/j.1365-2818.2009.03314.x.
- Woith, H., Petersen, G. M., Hainzl, S., and Dahm, T. (2018). Review: can animals predict earthquakes? *Bull. Seismol. Soc. Am.* 108, (3A), 1031–1045. doi:10.1785/0120170313
- Zafir, H. (2007). “The diurnal, multiday and seasonal evolution of Rn-222 within rocks along the Dead Sea Transform in relevance to earthquakes related phenomena,” in *Eos Trans. AGU* 88 (52), Fall meeting Suppl. Abstract T43A-1080.
- Zafir, H. (2008). The evolution, transportation and variation in time of Rn-222 within rocks in a desert region. *Geophys. Res. Abstr.* 10, 2008 EGU2008-A-05386.
- Zafir, H., Barbosa, S. M., and Malik, U. (2013). Differentiation between the effect of temperature and pressure on radon within the subsurface geological media. *Radiat. Meas.* 49, 39–56. doi:10.1016/j.radmeas.2012.11.019
- Zafir, H., Ben Horin, Y., Malik, U., Chemo, C., and Zalevsky, Z. (2016). Novel determination of radon-222 velocity in deep subsurface rocks and the feasibility to using radon as an earthquake precursor. *J. Geophys. Res. Solid Earth.* 121, 6346–6364. doi:10.1002/2016JB013033
- Zafir, H., Ginzburg, B., Hrvoic, I., Shirman, B., Gazit-Yaari, N., Steinitz, G., et al. (2003). “Ultra-sensitive monitoring of the geomagnetic field combined with radon emanation as a tool for studying earthquake related phenomena.” in *AGU, Fall Meeting*, April 11, 2003, Available at: <https://ui.adsabs.harvard.edu/abs/2003AGUFM.T51E0206Z/abstract>.
- Zafir, H., Haquin, G., Malik, U., Barbosa, S. M., Piatibratova, O., and Steinitz, G. (2011). Gamma versus alpha sensors for Rn-222 long-term monitoring in geological environments. *Radiat. Meas.* 46, 611–620. doi:10.1016/j.radmeas.2011.04.027

- Zafir, H., and Malik, U. (2010). "The effect of climatic condition on radon-222 within subsurface media." in The 3rd Ra–Rn international workshop on "The Radium and Radon Isotopes as Environmental Tracers," Jerusalem, Israel, March 14–19, 2010.
- Zafir, H., Malik, U., Levintal, E., Weisbrod, N., Ben Horin, Y., Zalevsky, Z., et al. (2019). "Radon and CO₂ in deep, as a proxy for pre-seismic research," in 15th International conference on gas geochemistry ICGG15, Palermo & Milazzo, 30 September 5 October 2019.
- Zafir, H., Steinitz, G., Malik, U., Haquin, G., and Gazit-Yaari, N. (2009). Response of Radon in a seismic calibration explosion, Israel. *Radiat. Meas.* 44, 193–198. doi:10.1016/j.radmeas.2009.01.002

Conflict of Interest: The authors declare that the research was conducted in the absence of any commercial or financial relationships that could be construed as a potential conflict of interest.

Copyright © 2020 Zafir, Barbosa, Levintal, Weisbrod, Ben Horin and Zalevsky. This is an open-access article distributed under the terms of the Creative Commons Attribution License (CC BY). The use, distribution or reproduction in other forums is permitted, provided the original author(s) and the copyright owner(s) are credited and that the original publication in this journal is cited, in accordance with accepted academic practice. No use, distribution or reproduction is permitted which does not comply with these terms.